

**Reconstruction of the Greenland Ice Sheet surface  
mass balance and the spatiotemporal distribution of  
freshwater runoff from Greenland to surrounding seas**

SEBASTIAN H. MERNILD

*Nansen Environmental and Remote Sensing Center, Bergen, NORWAY, Direction of Antarctic  
and Sub-Antarctic Programs, Universidad de Magallanes, Punta Arenas, CHILE, and  
Department of Environmental Sciences, Western Norway University of Applied Sciences,  
Sogndal, NORWAY*

GLEN E. LISTON

*Cooperative Institute for Research in the Atmosphere, Colorado State University, Fort Collins,  
Colorado, USA*

ANDREW P. BECKERMAN

*Department of Animal and Plant Sciences, University of Sheffield, UK*

JACOB C. YDE

*Department of Environmental Sciences, Western Norway University of Applied Sciences,  
Sogndal, NORWAY*

*Submitted to The Cryosphere, October 15, 2017*

*Resubmitted April 10, 2018*

**Corresponding author address:**

Sebastian H. Mernild, e-mail: [sebastian.mernild@nersc.no](mailto:sebastian.mernild@nersc.no)

## Abstract

Knowledge about variations in runoff from Greenland to adjacent fjords and seas is important for the hydrochemistry and ocean research communities to understand the link between terrestrial and marine Arctic environments. Here, we simulate the Greenland Ice Sheet (GrIS) surface mass balance (SMB), including refreezing and retention, and runoff together with catchment-scale runoff from the entire Greenland landmass ( $n = 3,272$  simulated catchments) throughout the 35-year period 1979–2014. SnowModel/HydroFlow ~~was-is~~ applied at 3-h intervals to resolve the diurnal cycle and at 5-km horizontal grid ~~resolution increments~~ using ERA-Interim (ERA-I) reanalysis atmospheric forcing. Variations in meteorological and surface ice and snow cover conditions influenced the seasonal variability in simulated catchment runoff; variations in the GrIS internal drainage system ~~were-are~~ assumed negligible and a time-invariant digital elevation model ~~was-is~~ applied. Approximately 80 % of all catchments showed increasing runoff trends over the 35 years, with on average relatively high and low catchment-scale runoff from the SW and N parts of Greenland, respectively. Outputs from an Empirical Orthogonal Function (EOF) analysis ~~were-are~~ combined with cross-correlations indicating a direct link (zero lag time) between modeled catchment-scale runoff and variations in the large-scale atmospheric circulation indices North Atlantic Oscillation (NAO) and Atlantic Multidecadal Oscillation (AMO). This suggests that natural variabilities in AMO and NAO constitute ~~major~~ controls on catchment-scale runoff variations in Greenland.

**KEYWORDS:** Empirical Orthogonal Function; Greenland freshwater runoff; Greenland Ice Sheet; HydroFlow; Modeling; NASA MERRA; SnowModel; surface mass-balance

## 1. Introduction

The Greenland Ice Sheet (GrIS) is highly sensitive to changes in climate (e.g., Box et al. 2012; Hanna et al. 2013; Langen et al. 2015; Wilton et al. 2016; AMAP 2017). It is of scientific interest and importance because it constitutes a massive reserve of freshwater that discharges to adjacent fjords and seas (Cullather et al. 2016). Runoff from Greenland influences the sea surface temperature, salinity, stratification, marine ecology, and sea-level in a number of direct and indirect ways (e.g., Rahmstorf et al. 2005; Straneo et al. 2011; Shepherd et al. 2012; Weijer et al. 2012; Church et al. 2013; Lenaerts et al. 2015).

The GrIS surface mass balance (SMB) and freshwater runoff have changed over the last decades and most significantly since the mid-1990s (e.g., Church et al. 2013; Wilton et al. 2016). For example, recent estimates by Wilton et al. (2016) showed a decrease in SMB from ~350 Gt yr<sup>-1</sup> (early-1990s) to ~100 Gt yr<sup>-1</sup> (~~late-2000s~~in 2010–2012) and an increase in runoff from ~200 Gt yr<sup>-1</sup> (early-1990s) to ~450 Gt yr<sup>-1</sup> (~~late-2000s~~in 2010 and 2012). Van den Broeke et al. (2016) showed a decrease in SMB from 398 Gt yr<sup>-1</sup> (1961–1990) to 306 Gt yr<sup>-1</sup> (1991–2015) and an increase in runoff from 256 Gt yr<sup>-1</sup> (1961–1990) to 363 Gt yr<sup>-1</sup> (1991–2015). For 2009 through 2012, the runoff has been estimated to include approximately two-third of the gross GrIS mass loss (Enderlin et al. 2014), while the net GrIS mass loss, on average, was 375 Gt yr<sup>-1</sup> (2011–2014) (AMAP 2017). The contribution of GrIS mass loss to global mean sea-level was around 5 % in 1993, and more than 25 % in 2014 (Chen et al. 2017), and up to 43 % for the GrIS and - ~~Noël et al. (2017), however, estimated the GrIS and peripheral glaciers and ice caps in 2010–2012 (Noël et al. 2017), to contribute approximately 43 % to the contemporary sea level rise,~~

Runoff from the GrIS is an integrated response of rain, snowmelt, and glacier melt and other hydrometeorological processes (e.g., Bliss et al. 2014). Tedesco et al. (2016) estimated a

Formatted: Font: Font color: Black

73 1979–2016 change in GrIS spatial surface melt extent of  $\sim 15,820 \text{ km}^2 \text{ yr}^{-1}$ , and a change in  
74 ~~surface ablation~~melt season duration of  $\sim 30$ – $40$  days in NE and  $15$ – $20$  days along the west coast.  
75 At higher GrIS elevations, surface melt does not necessarily equal surface runoff because  
76 meltwater may be retained or refrozen ~~refreeze~~ in the porous near-surface snow and firn layers  
77 (Machguth et al. 2016), where the firn pore space provides potential storage for meltwater  
78 (Haper et al. 2012; van Angelen et al. 2013). Melt water percolation, refreezing, and  
79 densification processes are common in GrIS snow, firn, and multi-year firn layers – especially  
80 where semipermeable or impermeable ice layers are present (Brown et al. 2012; van As et al.  
81 2016). Such physical mechanisms and conditions in the firn and multi-year firn layers lead, e.g.,  
82 to non-linearity in meltwater retention (Brown et al. 2012).

83 The GrIS internal drainage system has received increased attention in recent years. This  
84 is, in part, because the summer acceleration of ice flow is controlled by supraglacial meltwater  
85 draining to the subglacial environment (Zwally et al. 2002; van de Wal et al. 2008; Shephard et  
86 al. 2009). Enhanced production of supraglacial meltwater results in more water supplied to the  
87 glacier bed, leading to reduced basal drag and accelerated basal ice motion. This process is  
88 referred to as basal lubrication, and it constitutes a potential positive feedback mechanism  
89 between climate change and sea-level rise (Hewitt 2013). At high GrIS elevations, surface  
90 meltwater primarily drains to the glacier bed via hydrofractures (van der Veen 2007), whereas  
91 meltwater is routed to the glacier bed via crevasses and moulins in the peripheral areas (Banwell  
92 et al. 2016; Everett et al. 2016; Koziol et al. 2017). Rapid drainage of large volumes of GrIS  
93 meltwater come from sudden release from supraglacial and proglacial lakes (known as a glacial  
94 lake outburst flood (GLOF) or jökulhlaup), which are particular~~ly~~ common in ~~W~~west Greenland  
95 (Selmes et al. 2011; Carrivick and Quincey 2014). The seasonal evolution of the structure and  
96 efficiency of the drainage system beneath the GrIS is indirectly assumed from our understanding

97 of the subglacial hydraulic potential beneath Alpine glaciers. This general understanding is used  
98 to explain the observed seasonal changes in ice motion (Bartholomew et al. 2010, 2012) where  
99 few direct observations exist (Kohler et al. 2017). In fact, we know very little about  
100 spatiotemporal shifts in the configuration of the subglacial drainage network beneath the GrIS.  
101 We therefore assume that the subglacial drainage network in the natural system is dynamic and  
102 sensitive to rerouting of water flow between adjacent catchments (so-called water piracy; Chu et  
103 al. 2016), although we do not understand the details sufficiently to implement them in a runoff  
104 routing model.

105 We also lack high resolution information on the spatiotemporal distribution of GrIS and  
106 Greenland freshwater runoff to the fjords and seas, and the spatiotemporal distribution of solid-  
107 ice discharge (calving) from tidewater glaciers is also largely unknown, even-although Enderlin  
108 et al. (2014) estimated solid-ice discharge from around 180 tidewater glaciers ~~(Howat et al.~~  
109 ~~2013)~~. To address this lack of knowledge, information about the quantitative discharge (runoff  
110 and solid-ice discharge) conditions from the numerous ~~of~~ catchments in Greenland is required.  
111 Available GrIS calving rates are insufficient to represent the calving rates from the entire  
112 Greenland and are therefore not generally included in overall Greenland freshwater estimates  
113 (Nick et al. 2009; Lenaerts et al. 2015). This is an unaddressed gap, which likely prevents us  
114 from comprehensively understanding the terrestrial freshwater discharge to the fjords and seas.  
115 This also limits the subsequent ~~the~~ link between changes in terrestrial inputs and changes in the  
116 hydrographic and circulation conditions. This ~~unaddressed knowledge gap~~ has further  
117 implications for ocean model simulations, where, for example, earlier representations of  
118 Greenland discharge boundary conditions were either non-existent or overly simplistic (e.g.,  
119 Weijer et al. 2012).

Previous GrIS studies constructed a section-wise runoff distribution by dividing the ice sheet into six to eight overall defined sections (e.g., Rignot et al. 2008; Bamber et al. 2012; Rignot and Mouginot 2012; Lenaerts et al. 2015; Wilton et al. 2016). These studies illustrated an increase in runoff since 1870 for all GrIS sections, with the greatest increase in runoff since mid-1990s and in the ~~SW~~southwestern part of the ice sheet.

Mernild and Liston (2012) reconstructed the GrIS SMB and the Greenland spatiotemporal runoff distribution from ~3,150 individually simulated catchments, at 5-km spatial, and daily temporal, resolutions covering the period from 1960 through 2010. Automatic weather stations located both on and off the GrIS were used for atmospheric forcings in Mernild and Liston (2012). ~~and~~ The study was carried out using a full energy balance, multi-layer snowpack and snow distribution, and freshwater runoff model and a software package called SnowModel/HydroFlow (Liston and Elder 2006a; Liston and Mernild 2012). These individual catchment outlet runoff time series were analyzed to map runoff magnitudes and variabilities in time, but also emphasized trends and spatiotemporal variations, including runoff contributions from the GrIS, the land area (the tundra region) between the GrIS ice margin and the ocean, from the relatively small isolated glaciers and ice caps, and from entire Greenland. This approach is especially important when trying to understand the total runoff fraction from Greenland, including the annual and seasonal freshwater runoff variabilities within individual catchments.

Here, we improve the work by Mernild and Liston (2012) by using ~~an updated version of~~ SnowModel/HydroFlow and by including a new digital elevation model (DEM). We also extend the time series to 2014 by using the ERA-Interim (ERA-I) reanalysis products on 3-h time step (Dee et al. 2011). The objective of this study is to simulate, map, and analyze first-order atmospheric forcings and GrIS mass balance components for Greenland. The analyzed variables

include the GrIS SMB, together with GrIS surface air temperature, surface melt, precipitation, evaporation, sublimation, refreezing and retention, and surface freshwater runoff and specific runoff (runoff volume per time per unit drainage area,  $L s^{-1} km^{-2}$ ; to convert to  $mm yr^{-1}$ , multiply by 31.6)~~conditions~~. The time period covers 1979–2014 (35 years), with a focus on the present day conditions 2005–2014 ~~(the last decade of the simulations)~~. Further, the spatiotemporal magnitude, distribution, and trends of individual catchment-scale runoff and specific runoff from Greenland ( $n = 3,272$ ; where  $n$  is the number of simulated catchments, each with an individual flow network) were simulated based on HydroFlow-generated watershed divides and flow networks for each catchment. The simulated spatiotemporal catchment-scale outlet runoff is useful as boundary conditions for fjord and ocean model simulations. We also analyzed the spatiotemporal catchment-scale outlet runoff using Empirical Orthogonal Functions (EOF). This analysis allowed us to describe simultaneously how the spatial patterns of catchment-scale outlet runoff changed over time. It also allowed us to explore via cross-correlations the relationship between the spatiotemporal patterns of runoff and large-scale atmospheric-ocean circulation indices including the North Atlantic Oscillation (NAO) and the Atlantic Multidecadal Oscillation (AMO), with particular attention to the lag-times, if any, between variations in NAO and AMO and responses in Greenland catchment-scale runoff.

## 2. Model description, setup, and ~~evaluation~~verification

### 2.1 *SnowModel*

*SnowModel* (Liston and Elder 2006a) is established by six sub-models, where five of the models were used here to quantify spatiotemporal variations in atmospheric forcing, surface snow properties, GrIS SMB, and Greenland catchment runoff. The sub-model *MicroMet* (Liston

and Elder 2006b; Mernild et al. 2006a) downscaled and distributed the spatiotemporal atmospheric fields using the Barnes objective interpolation scheme. Interpolation fields were adjusted, where the interpolated fields subsequent were adjusted using known meteorological algorithms, e.g., temperature-elevation, wind-topography, humidity-cloudiness, and radiation-cloud-topography relationships (Liston and Elder 2006b). *Enbal* (Liston 1995; Liston et al. 1999) simulated a full surface energy balance considering the influence of cloud cover, sun angle, topographic slope, and aspect on incoming solar radiation, and moisture exchanges, e.g., multilayer heat- and mass-transfer processes within the snow (Liston and Mernild 2012). *SnowTran-3D* (Liston and Sturm 1998, 2002; Liston et al. 2007) accounted for the snow (re)distribution by wind. *SnowPack-ML* (Liston and Mernild 2012) simulated multilayer snow depths, temperatures, and density evolutions~~water equivalent evolutions~~. *HydroFlow* (Liston and Mernild 2012) simulated watershed divides, routing network, flow residence-time, and runoff routing (configurations based on the ~~hypothetical~~-gridded topography~~), and ocean mask datasets~~), and discharge hydrographs for each grid cell including ~~from~~ catchment outlets. These sub-models have been ~~tested~~-evaluated against independent observations with success in Greenland, Arctic, high mountain regions, and on the Antarctic Ice Sheet with acceptable results (e.g., Hiemstra et al. 2006; Liston and Hiemstra 2011; Beamer et al. 2016). For detailed information regarding the use of SnowModel for the GrIS<sup>2</sup> or local Greenlandic glaciers<sup>2</sup> SMB and runoff simulations, we refer to Mernild and Liston (2010, 2012) and Mernild et al. (2010a, 2014).

## 2.2 Meteorological forcing, model configuration and model limitations

SnowModel was forced with ERA-Interim (ERA-I) reanalysis products on a  $0.75^\circ$  longitude  $\times$   $0.75^\circ$  latitude grid from the European Centre for Medium-Range Weather Forecasts



(ECMWF; Dee et al. 2011). The simulations were conducted from 1 September 1979 through 31 August 2014 (35 years) (henceforth 1979–2014), where the 6-hour (precipitation at 12-hour) temporal resolution ERA-I data was downscaled to 3-hourly values ~~and on~~ a 5-km grid using MicroMet. The 6-hour data were scaled to 3-hours by linear interpolation, and the 12-hour precipitation was equally distributed over the 3-hour intervals for the last 12 hours. The 3-hour temporal resolution was chosen to allow SnowModel to resolve the solar radiation diurnal cycle in its simulation of snow and ice temperature evolution and melt processes.

The DEM was obtained from Levinsen et al. (2015) (original resolution  $2 \times 2$  km;  $4 \text{ km}^2$ ), and rescaled to a 5-km horizontal grid ~~increment-resolution~~ that covered the GrIS (1,646,175  $\text{km}^2$ ), mountain glaciers, and the entire Greenland (2,166,725  $\text{km}^2$ ) and the surrounding fjords and seas (Figure 1a). The DEM is time-invariant specific to the year 2010. The DEM was developed by merging contemporary radar and laser altimetry data, where radar data were acquired with Envisat and CryoSat-2, and laser data with the Ice, Cloud, and land Elevation Satellite (ICESat), the Airborne Topographic Mapper (ATM), and the Land, Vegetation, and Ice Sensor (LVIS). Radar data were corrected for horizontal, slope-induced, and vertical errors from penetration of the echoes into the subsurface (Levinsen et al. 2015). Since laser data are not subject to such errors, merging radar and laser data yields a DEM that resolves both surface depressions and topographic features at higher altitudes (Levinsen et al. 2015). The distribution of glacier cover was obtained from the Randolph Glacier Inventory (RGI, v. 5.0) polygons; these data were resampled to the 5-km grid. The SnowModel land-cover mask defined glaciers to be present when individual grid cells were covered by 50 % or more ~~of~~ with glacier ice.

In MicroMet, only one-way atmospheric coupling was provided, where the meteorological conditions were prescribed at each time step. In the natural system, the

atmospheric conditions would be adjusted in response to changes in surface conditions and properties (Liston and Hiemstra 2011). Due to the use of the 5-km horizontal grid increments, snow transport and blowing-snow sublimation processes (usually produced by SnowTran-3D in SnowModel) were excluded from the simulations because blowing snow does not typically move completely across 5-km distances (Liston and Sturm 2002; Mernild et al. 2017). Static sublimation was, however, included in the model integrations. In HydroFlow, the generated catchment divides and flow network were controlled by the DEM, i.e., exclusively by the surface topography and not by the development of the glacial drainage system. The role of GrIS bedrock topography on controlling the potentiometric surface and the associated meltwater flow direction was assumed to be a secondary control on discharge processes (Cuffey and Paterson 2010).

Formatted: Not Highlight

First, the GrIS DEM was initially divided into six major sections following Rignot et al. (unpublished): southwest (SW), west (W), northwest (NW), north (N), northeast (NE), and southwest (SW) (Figure 1b and Table 1). Second, HydroFlow divided Greenland into 3,272 individual catchments (Figure 1c), each with an eight-compass-direction water-flow network where water is transported through this network via linear reservoirs. Only a single outlet into the seas was allowed for each individual catchment.

The mean and median catchment sizes were 680 km<sup>2</sup> and 75 km<sup>2</sup>, respectively. The top one percent of the largest catchments accounted for 53 % of the Greenland area. This distribution of HydroFlow-defined GrIS catchments (Figure 1c) closely matched both the catchment distribution by Mernild and Liston (2012) and by Rignot and Kanagaratnam (2006) for the 20 largest GrIS catchments (not including midsize and minor catchments), both with respect to size and location of the watershed divide. The total number of HydroFlow-generated catchments

presented in this study was ~4 % higher due to the use of the DEM obtained from Levinsen et al. (2015), than the number of Greenland catchments in the Mernild and Liston (2012) study.

~~In MicroMet, only one-way atmospheric coupling was provided, where the meteorological conditions were prescribed at each time step. In the natural system, the atmospheric conditions would be adjusted in response to changes in surface conditions and properties (Liston and Hiemstra 2011). Due to the use of the 5-km horizontal grid increments, snow transport and blowing-snow sublimation processes (usually produced by SnowTran-3D in SnowModel) were excluded from the simulations because blowing snow does not typically move completely across 5-km distances. Static sublimation was, however, included in the model integrations. In HydroFlow, the generated catchment divides and flow network were controlled by the DEM, i.e., exclusively by the surface topography and not by the development of the glacial drainage system. The role of GrIS bedrock topography on controlling the potentiometric surface and the associated meltwater flow direction was assumed to be a secondary control on discharge processes (Cuffey and Paterson 2010).~~

An example of the HydroFlow generated catchment divides and flow network is illustrated in detail by Mernild et al. (2018; Figure 1c) for the Kangerlussuaq catchment in central West Greenland, ~~which includes a part of the GrIS~~ (67°N, 50°W; SW sector of the GrIS). The same catchment from where SnowModel/HydroFlow was evaluated against independent observations (see Section 2.3). Because the DEM is time-invariant, no changes ~~though feedbacks~~ from a thinning ice, ice retreat, and from changes in hypsometry will influence the catchment divides and the flow network patterns, including the glacial drainage system. Changes in runoff over time are therefore solely influenced by the climate signal and the surface snow and ice cover conditions (runoff was generated from gridded inputs from rain, snowmelt,

Formatted: Not Highlight

Formatted: Not Highlight

257 and ice melt), ~~not by the glacial drainage system~~. In HydroFlow, the meltwater flow velocities  
258 were ~~gained~~ obtained from dye tracer experiments conducted both through the snowpack (in  
259 early and late-summer) and through the englacial and subglacial environments (Mernild et al.  
260 2006b).

### 262 2.3 ~~Verification~~ Evaluation

263 For Greenland, long-term catchment river runoff observations are sparse; at present  
264 ~~approximately ten~~ at least eight permanent hydrometric monitoring stations are operating  
265 (Mernild 2016), measuring the sub-daily and sub-seasonal runoff variability originating from  
266 rain, melting snow, and melting ice from local glaciers and the GrIS. In addition, these  
267 observations only span parts of the runoff season, ranging between few weeks to approximately  
268 three months. For the Kangerlussuaq area, independent meteorological, ~~and~~ snow and ice  
269 observational, and river runoff datasets are also available, e.g., K-transect point observed air  
270 temperature, and SMB and catchment outlet observed ~~discharge~~ runoff (discharge) from Watson  
271 River (e.g., van de Wal et al. 2005; van den Broeke et al. 2008a; 2008b, Hasholt et. al. 2013, van  
272 As et al. 2018). These observed datasets were used for ~~verification~~ evaluation of the  
273 SnowModel/HydroFlow ERA-I simulated GrIS mean annual air temperature (MAAT), ~~GrIS~~  
274 SMB, ELA (equilibrium-line altitude: the spatially averaged elevation of the equilibrium line,  
275 defined as the set of points on the glacier surface where the net mass balance is zero), and  
276 catchment river outlet freshwater runoff presented herein (Mernild et al. ~~2017~~ 2018). These  
277 model ~~verifications~~ evaluations showed acceptable results for the Kangerlussuaq area,  
278 illustrating a difference between observations and simulations, for example, in MAAT of 0.2–  
279 0.5°C (1993–2014), and in GrIS SMB of  $0.17 \pm 0.23$  m w.e. (1990–2014), where the  $r^2$ -value

Formatted: Font: (Default) Times New Roman, 12 pt, Not Highlight

Formatted: Not Highlight

Formatted: Not Highlight

Formatted: Font: (Default) Times New Roman, 12 pt

Formatted: Not Highlight

Formatted: Not Highlight

Formatted: Font: (Default) Times New Roman, 12 pt

Formatted: Not Highlight

Formatted: Font: (Default) Times New Roman, 12 pt

Formatted: Not Highlight

Formatted: Font: Italic

Formatted: Font: Italic, Superscript

280 ~~(where  $r^2$  is the explained variance)~~ ranged between 0.55 and 0.67 (linear), except for one AWS  
 281 in the K-Transect where  $r^2$  was 0.28 (AWS S6). The simulated Kangerlussuaq mean GrIS ELA  
 282 (1979–2014) was located at  $1,760 \pm 260$  m a.s.l. In van As et al. (2018<sup>7</sup>), the ELA was defined  
 283 as the altitude where SMB minus refreezing equals zero, and it was to be located at  
 284 approximately 1,800 m a.s.l. (2009–2015), and in van de Wal et al. (2012) ELA was estimated  
 285 to at approximately 1,610 m a.s.l. (1991–2014) (for further information see Mernild et al.  
 286 2018<sup>7</sup>). ~~Regarding, s~~ Simulated Kangerlussuaq catchment river outlet runoff it was, however, on  
 287 average overestimated by  $31 \pm 9$  % (2007–2013) and subsequently adjusted against observed  
 288 runoff ( $r^2 = 0.76$  (linear); for further information see Mernild et al. 2018). This freshwater runoff  
 289 overestimation is ~~could likely related to the be because of~~ missing multiyear firn processes in  
 290 SnowModel, such as nonlinear meltwater retention, percolation blocked by ice layers, and  
 291 refreezing. Due to the limited long-term river runoff observations from the GrIS, the  
 292 Kangerlussuaq runoff adjustment from Mernild et al. (2018) was used herein for the entire GrIS.  
 293 The adjusted GrIS runoff is henceforth referred to as runoff.

294 Further, ~~The the~~ use of ERA-I has also showed promising results after a full evaluation  
 295 estimating changes in ice sheet ~~surface mass balance~~ SMB for the catchments linked to  
 296 Godthåbsfjord (64° N) in Southwest Greenland (Langen et al. 2015).

297 In the analysis that follows, all correlation trends declared ‘significant’ are statistically  
 298 significant at or above the 5 % level ( $p < 0.05$ ; based on a linear regression  $t$  test).

## 299 2.4 Surface water balance components

301 For the GrIS, surface water balance components can be estimated using the hydrological  
 302 method (continuity equation) (Equation 1):

Formatted: Not Highlight

Formatted: Font: (Default) Times New Roman, 12 pt

Formatted: Font: (Default) Times New Roman, 12 pt, Italic

Formatted: Font: (Default) Times New Roman, 12 pt, Italic, Superscript

Formatted: Font: (Default) Times New Roman, 12 pt

Formatted: Font: Italic

Formatted: Font: Italic, Superscript

Formatted: Not Highlight

Formatted: Not Highlight

Formatted: Font: (Default) Times New Roman, 12 pt

Formatted: Font: (Default) Times New Roman, 12 pt

Formatted: Font: (Default) Times New Roman, 12 pt

Formatted: Font: (Default) Times New Roman, 12 pt

Formatted: Font: (Default) Times New Roman, 12 pt

Formatted: Font: (Default) Times New Roman, 12 pt

Formatted: English (United States)

Formatted: Font: (Default) Times New Roman, 12 pt

Formatted: Font: (Default) Times New Roman, 12 pt

Formatted: Font: (Default) Times New Roman, 12 pt

Formatted: Font: (Default) Times New Roman, 12 pt

Formatted: Font: (Default) Times New Roman, 12 pt

Formatted: Font: (Default) Times New Roman, 12 pt

Formatted: Font: (Default) Times New Roman, 12 pt

Formatted: Font: (Default) Times New Roman, 12 pt

Formatted: Font: (Default) Times New Roman, 12 pt

Formatted: Font: (Default) Times New Roman, 12 pt

Formatted: Font: (Default) Times New Roman, 12 pt

Formatted: Not Highlight

Formatted: Font: (Default) Times New Roman, 12 pt

Formatted: Font: Italic

Formatted: Font: Italic, Superscript

Formatted: Font: (Default) Times New Roman, 12 pt

Formatted: Font: (Default) Times New Roman, 12 pt

Formatted: Font: (Default) Times New Roman, 12 pt

Formatted: Font: (Default) Times New Roman, 12 pt

Formatted: Font: (Default) Times New Roman, 12 pt

Formatted: Font: (Default) Times New Roman, 12 pt

Formatted: Font: (Default) Times New Roman, 12 pt

Formatted: Highlight

303

304 
$$P - (Su + E) - R + \Delta S = 0 \pm \eta, \quad (1)$$

305

306 where  $P$  is precipitation input from snow and rain,  $Su$  is sublimation from a static surface,  $E$  is  
307 evaporation,  $R$  is runoff from snowmelt, ice melt, and rain,  $\Delta S$  is change in storage ( $\Delta S$  is also  
308 referred to as SMB) derived as the residual value from changes in glacier and snowpack storage.  
309 For snow and ice surfaces, the ablation was estimated as:  $Su + E + R$ . The amount of snow  
310 refreezing and retention was estimated as:  $P_{rain} + melt_{surface} - R$  (for bare ice:  $P_{rain} + melt_{surface} =$   
311  $R$ ). The parameter  $\eta$  is the water balance discrepancy. This discrepancy should be 0 (or small), if  
312 the components  $P$ ,  $Su$ ,  $E$ ,  $R$ , and  $\Delta S$  have been determined accurately.

313

### 314 **3. EOF runoff analysis**

315 We applied an Empirical Orthogonal Function (EOF) analysis to define the  
316 spatiotemporal pattern in simulated catchment outlet runoff. EOF is a statistical tool that  
317 analyzes spatial and temporal runoff data to find combinations of locations that vary consistently  
318 through time, and combinations of time, that vary in a spatially consistent manner (e.g.,  
319 Preisendorfer 1998; Sparnocchia et al. 2003). The major axes of the EOF analysis identify  
320 variations in the catchment outlet runoff in both time and space.

321 The eigenvalues of the EOFs can be correlated with the temporal data, and the  
322 eigenvectors with spatial locations, to identify how the EOF describes change in runoff in time  
323 and across space. Furthermore, the temporal patterns embedded in the EOFs can, via cross-  
324 correlation analysis, be related to larger scale atmospheric-ocean indices (Mernild et al. 2015), in  
325 this case the North Atlantic Oscillation (NAO) and Atlantic Multi-decadal Oscillation (AMO).

The NAO and AMO indices were obtained from Hurrell and van Loon (1997) and Kaplan et al. (1998), respectively. This latter analysis enables to link change fluctuations in can generate hypotheses about whether, for example, NAO or AMO to with GrIS catchment mass-loss and outlet river runoff leads by some years changes in mass balance and runoff (the lag in the cross-correlation analyses tells us these details).

We focused on the NAO and AMO for several reasons. NAO is estimated based on the mean sea-level pressure difference between the Azores High and Icelandic Low. NAO is a large-scale atmospheric circulation index, and is therefore a good measure of airflow and jet-stream moisture transport variability (e.g., Overland et al. 2012) from the North Atlantic onto Northwest Europe (Dickson et al. 2000; Rogers et al. 2001). According to Hurrell (1995), a positive NAO is associated with cold conditions in Greenland, while a negative NAO corresponds to mild conditions. AMO is a large-scale oceanic circulation index, and an expression of fluctuating mean sea-surface temperatures in the North Atlantic (Kaplan et al. 1998). For example, Arctic land surface air temperatures are highly correlated with the AMO (Chylek et al. 2010), and the overall annual trend in the mean GrIS melt extent correlates with the smoothed trends of the AMO (Mernild et al. 2011). A positive AMO indicates relatively high surface air temperature and less precipitation at high latitudes (relatively high net mass balance-loss), whereas a negative AMO indicates relatively low surface air temperature and a higher precipitation (relatively low net mass balance loss) (Kaplan et al. 1998).

## 4. Results and discussion

### 4.1 GrIS surface water balance conditions

Figure 2 presents the SnowModel ERA-I simulated 35-year mean spatial GrIS surface MAAT, precipitation, surface melt, evaporation and sublimation, ablation, and SMB. Overall, all variables follow the expected spatial patterns. For example, the lowest MAAT occurred at the GrIS interior ( $\leq -27^{\circ}\text{C}$ ) and highest values were at the margin ( $\geq 0^{\circ}\text{C}$ ). Also, the lowest annual mean precipitation values were situated in the northern half of the GrIS interior ( $\leq 0.25$  m water equivalent (w.e.)), while peak values occurred in the southeastern part of Greenland ( $\geq 3.5$  m w.e.). The lowest annual mean surface melt values ( $\leq 0.0625$  m w.e.) were present at the upper parts of the GrIS and vice versa at the lowest margin areas ( $\geq 5.0$  m w.e.). The 35-year mean SMB illustrated net loss at the lowest elevations of  $\geq 3.54\text{-}0$  m w.e. and net gain at the highest elevations of between 0 and 0.25 m w.e. The peak net gain of  $\geq 3.5\text{-}0$  m w.e. occurred in Southeast Greenland, which matches what is generally expected from the overall precipitation pattern over the GrIS. The SnowModel ERA-I spatial simulated 35-year mean distributions generally agree with previous studies by Fettweis et al. (2008, 2017), Hanna et al. (2011), and Box (2013), within the different temporal domains covered by these studies.

On GrIS section-scale (Table 1), a clear variability between the six sections (Figure 1b) occurred for the surface mass-balance components (Equation 1) for both the 35-year mean and the last decade. On average, most precipitation fell in the Southeast Greenland sector of  $242.6 \pm 39.1$  Gt  $\text{yr}^{-1}$  (where,  $\pm$  equals one standard deviation). This was likely due to the cyclonicity between Iceland and Greenland, which typically sets up a prevailing easterly airflow towards the steep slopes of the southern coast of Greenland, generating orographic enhancement ~~southeastern coast of Greenland that includes orographic enhancement~~ (Hanna et al. 2006; Bales et al. 2009). The lowest 35-year mean precipitation of  $31.1 \pm 5.4$  Gt  $\text{yr}^{-1}$  occurred in the dry North Greenland. For the last decade, the mean annual precipitation was  $232.4 \pm 25.2$  Gt  $\text{yr}^{-1}$  and  $30.9 \pm 5.1$  Gt  $\text{yr}^{-1}$

Formatted: Not Highlight



for Southeast Greenland and North Greenland, respectively. This regional distribution is in accordance with the study on Greenlandic precipitation patterns by Mernild et al. (2015), although their analysis was based on observed precipitation from 2001–2012. Further, in Mernild et al. (2018; Figure 6b), the mean ERA-I grid point precipitation (located closest to the center of the Kangerlussuaq watershed) was tested against Kangerlussuaq SnowModel ERA-I downscaled mean catchment precipitation conditions; this analysis indicated no significant difference between the two datasets.

The ratio between rain and snow precipitation varied from <1 % (Northeast section) to 5 % (Southwest section), averaging 2 % and indicating that rain only played a minor role in the GrIS precipitation budget (Table 1). For the last decade, the average rainfall-to-snowfall ratio was 3 % for the entire GrIS.

For the GrIS, the overall precipitation was  $653.9 \pm 66.4$  Gt yr<sup>-1</sup> (35 years) and  $645.0 \pm 39.0$  Gt yr<sup>-1</sup> (2005–2014), which is within the lower range of previously reported values (Fettweis et al. 2017; Table 1). For example, in MAR (Modèle Atmosphérique Régional; v. 3.5.2) the simulated precipitation was between ~~642.0 and 747.0~~ 642.747.0 Gt yr<sup>-1</sup> (1980–1999; snowfall plus rainfall) forced with a variety of forcings, e.g., ERA-40 (Uppala et al. 2005), ERA-I (Dee et al. 2011), JRA-55 (Japanese 55-year Reanalysis; Kobayashi et al. 2015).

As shown by Fettweis et al. (2017), precipitation is the parameter with the largest uncertainty due to the spread among the different forcing datasets. Also, systematic observational errors may occur during precipitation monitoring, such as wind-induced undercatch, because of turbulence and wind field deformation from the precipitation gauge, wetting losses, and trace amounts (e.g., Goodison et al. 1989; Metcalfe et al. 1994; Yang et al. 1999; Rasmussen et al. 2012). This highlights the importance of accurately representing precipitation for estimating the

~~energy~~ An understanding of precipitation conditions and uncertainties are therefore highly relevant for estimating the energy and moisture balances, surface albedo, GrIS SMB conditions, and, in a broader perspective, the GrIS's contribution to sea-level changes.

Besides precipitation, melt (including extent, intensity, and duration) and ablation are other relevant parameters for estimation and understanding GrIS ~~SMB, surface conditions, where~~ Surface melt can influence albedo, as wet snow (~~including extent, intensity, and duration~~) is relevant for SMB conditions. An altered surface melt regime can influence surface albedo, ~~because wet snow~~ absorbs up to three times more incident solar energy than dry snow (Steffen 1995), and the energy and moisture balances. Changes in the amount of meltwater also affect total runoff, but also ice dynamics, and subglacial lubrication and sliding processes (Hewitt 2013).

Surface melt varied on a section-scale, for the 35-year mean, from  $57.2 \pm 24.1$  Gt yr<sup>-1</sup> in North Greenland to  $155.2 \pm 48.4$  Gt yr<sup>-1</sup> in Southwest Greenland (Table 1). The average for the entire GrIS was  $542.9 \pm 175.3$  Gt yr<sup>-1</sup> (Table 1). During the last decade, the surface melt for the GrIS had increased to  $713.4 \pm 138.6$  Gt yr<sup>-1</sup>, varying from  $75.9 \pm 26.9$  Gt yr<sup>-1</sup> in ~~the N~~the northeast of Greenland to  $202.4 \pm 39.2$  Gt yr<sup>-1</sup> in Southwest Greenland. This is an increase of 31 % for the last decade compared to the entire simulation period, which was likely due to increasing MAAT (assuming an empirical relationship between air temperature (sensible heat) and surface melt rates) throughout the simulation period (Hanna et al. 2012).

The GrIS ablation patterns varied as expected between the northern and ~~southern~~ southwestern sections from  $50.265.7 \pm 15.622.6$  Gt yr<sup>-1</sup> in the north to ~~432.9 98.1~~  $29.2 42.2$  Gt yr<sup>-1</sup> in the south~~west~~. For the entire GrIS, the mean annual ablation was ~~400.9 530.3~~  $106.2153$  Gt yr<sup>-1</sup> and ~~687.8 510.0~~  $418.881.7$  Gt yr<sup>-1</sup> for the 35-year period and 2005–2014, respectively.

417 This was equal to an increase of ~~30.28~~ %, which was also reflected in the differences in  
418 variability from ~~83.362.3~~  $\pm$  ~~24.717.0~~ Gt yr<sup>-1</sup> in North Greenland to ~~175.1127.3~~  $\pm$  ~~35.223.9~~ Gt yr<sup>-1</sup>  
419 in Southwest Greenland (Table 1).

Formatted: Not Highlight

Formatted: Not Highlight

Formatted: Not Highlight

Formatted: Not Highlight

Formatted: Not Highlight

420 Runoff is a part of the ablation budget and therefore must be quantified to understand  
421 GrIS mass balance changes. Runoff varied from ~~50.034.5~~  $\pm$  ~~22.715.7~~ Gt yr<sup>-1</sup> in North Greenland  
422 to ~~112.677.7~~  $\pm$  ~~41.828.9~~ Gt yr<sup>-1</sup> in South~~west~~ Greenland, averaging ~~418.1288.7~~  $\pm$  ~~151.1104.3~~ Gt  
423 yr<sup>-1</sup> for the 35-year mean period over the GrIS. For 2005–2014, the mean runoff was ~~73.7395.4~~  $\pm$

Formatted: Not Highlight

424 ~~119.882.7~~ Gt yr<sup>-1</sup>; a 37 % increase (Table 1). For the period 1991–2015 van den Broeke et al.  
425 (2016) estimated on average the GrIS runoff to 363  $\pm$  102 Gt yr<sup>-1</sup>. This-The increase in  
426 SnowModel simulated GrIS runoff over time confirms the results from previous studies (e.g.,  
427 van den Broeke et al. 2016, Wilton et al. 2016). On a regional-scale, runoff varied from ~~67.646.6~~  
428  $\pm$  ~~25.017.3~~ Gt yr<sup>-1</sup> in North Greenland to ~~154.4106.6~~  $\pm$  ~~36.325.0~~ Gt yr<sup>-1</sup> in Southwest Greenland.

Formatted: Not Highlight

Formatted: Not Highlight

Formatted: Not Highlight

Formatted: Not Highlight

429 The simulated section runoff distribution was largely in agreement with trends noted by Lewis  
430 and Smith (2009) and Mernild and Liston (2012). The section runoff variability roughly followed  
431 the precipitation patterns, where sections with high precipitation equaled low runoff (e.g., in  
432 Southeast Greenland) and vice versa (e.g., in Southwest Greenland). More specifically, GrIS  
433 snowpack retention and refreezing processes suggest that sections with relatively high surface  
434 runoff were synchronous with relatively low end-of-winter snow accumulation because more  
435 meltwater was retained in the thicker, colder snowpack, reducing and delaying runoff to the  
436 internal glacier drainage system (e.g., Hanna et al. 2008). However, in maritime regions such as  
437 Southeast Greenland, high surface runoff can result from abnormally wet conditions (Mernild et  
438 al. 2014). Furthermore, runoff was negatively correlated to surface albedo and snow cold  
439 content, as confirmed by Hanna et al. (2008) and Ettema et al. (2009).

For the dry North and Northeast Greenland (Table 1), the relatively low end-of-winter snowpack melted relatively fast during spring warm-up. After the winter snowpack had ablated, the ice surface albedo promoted a stronger radiation-driven ablation and surface runoff, owing to the lower ice albedo. For the wetter Southeast Greenland (Table 1), the relatively high end-of-winter snow accumulation, combined with frequent summer snow precipitation events, kept the albedo high. Therefore, in that region ~~the snowpack persists longer compared to it generally took longer time to melt the snowpack compared to~~ the drier parts of the GrIS before ablation started to affect the underlying glacier ice.

Regarding specific runoff (runoff volume per unit drainage area per time,  $\text{L s}^{-1} \text{ km}^{-2}$ ; to convert to  $\text{mm yr}^{-1}$ , multiply by 31.6), maximum values of ~~46.7~~11.5  $\text{L s}^{-1} \text{ km}^{-2}$  and ~~22.9~~15.8  $\text{L s}^{-1} \text{ km}^{-2}$  were seen in Southwest Greenland for the mean 35-year and 2005–2014 periods, respectively. The minimum values of ~~4.4~~3.0  $\text{L s}^{-1} \text{ km}^{-2}$  and ~~6.2~~4.3  $\text{L s}^{-1} \text{ km}^{-2}$  for the mean 35-year and 2005–2014 periods, respectively, occurred in Northeast Greenland (Table 2). On average for the GrIS, the corresponding specific runoffs were ~~8.1~~5.6  $\text{L s}^{-1} \text{ km}^{-2}$  and ~~11.1~~7.6  $\text{L s}^{-1} \text{ km}^{-2}$ , respectively, which are within the range of ~~our previous study~~ previous studies (e.g., Mernild et al. 2008). Specific runoff is a valuable tool for comparing runoff on regional and catchment scales, ~~where regions and catchments varies in size, and it can also be used to quantifying the absolute runoff contributions from increasing runoff and increasing melt area extent. The difference in specific runoff between the two periods indicates that the increase in runoff has increased faster than the increase in melt area extent.~~

Refreezing and retention in the snow and firn packs were defined as rain plus surface melt minus runoff (see Section 2.4). For the GrIS, the 35-year mean refreezing and retention was estimated to be ~~25.49~~ % (~~140.1~~269.9  $\pm$  ~~35.5~~77.4  $\text{Gt yr}^{-1}$ ), and it was ~~2245~~ % (~~158.4~~318.0  $\pm$

34.462.8 Gt yr<sup>-1</sup>) for 2005–2014 (Table 1). Hence, refreezing and retention provided an important quantitative contribution to the evolution of snow and firn layers, ice densities, snow temperatures (cold content or snow temperatures below freezing), and moisture available for runoff (Liston and Mernild 2012). The SnowModel ERA-I refreezing and retention simulations were within the order of magnitude (~45 %) produced by the single layer snowpack model used by Hanna et al. (2008), but lower than the 45 % simulated by Noël et al. (2017) and Steger et al. (2017), where Steger et al. (2017) showed values in the range between 216–242 Gt yr<sup>-1</sup> (1960–2014). Ettema et al. (2009), Vizcaino et al. (2013), however, indicated refreezing values representing 35% of the available liquid water (the sum of rain and melt). On the regional-scale for the GrIS, the 35-year mean refreezing and retention value varied from 1340 % in North Greenland to 5730 % in both Southeast and Southwest Greenland. For 2005–2014, the values were 1239 % for North Greenland and 3257 % for Southeast Greenland (Table 1), indicating a clear variability in refreezing and retention between the different regions.

In Figure 3a, the time series of GrIS mean annual refreezing and retention shows an increasing trend (significant) and variability ranging from -0.0507 m w.e. (1992) to -0.1429 m w.e. (2012), with an annual mean value of 0.0916 ± 0.042 m w.e. In Figure 3b, the spatial 35-year mean GrIS refreezing and retention is presented together with values from 1992 and 2012, the minimum and maximum years, respectively. The mean spatial distribution highlights minimal refreezing and retention at the GrIS interior, whereas areas with low elevation had values above 0.758 m w.e. in southern part of the GrIS. For the minimum year 1992, the pattern was more pronounced with no refreezing and retention in the interior. The maximum year 2012 on the other hand had refreezing and retention at the interior (between 0 and 0.025 m w.e.) (Figure 3b). This was likely due to the extreme GrIS surface melt event throughout July 2012

Formatted: Font: (Default) Times New Roman, 12 pt, Not Highlight

Formatted: Font: (Default) Times New Roman, 12 pt, Not Highlight

Formatted: Font: (Default) Times New Roman, 12 pt, English (United States), Not Highlight

Formatted: Font: (Default) Times New Roman, 12 pt

(e.g., Nghiem et al. 2012; Hanna et al. 2014). When divided into regions and catchments, the 2012 simulated refreezing and retention showed a clear separation between highest values in Southwest Greenland and lowest values in Northeast and East Greenland. Because here, refreezing and retention were estimated as the sum of rain and melt minus the sum of runoff, this SnowModel analysis did not provide a detailed description of the physical mechanisms and conditions (beyond the standard SnowModel snowpack temperature and density evolution) leading to, e.g., non-linearities in snow and firn meltwater retention (Brown et al. 2012). However, while likely an oversimplification of the natural system, this quantitative estimation of refreezing and retention is an important step forward, and improves our runoff and the associated SMB estimates. A model that does not include refreezing and retention processes in its snow and firn evolution calculations, and the associated impacts on SMB, will introduce additional uncertainty in its calculations of GrIS SMB and its contribution to sea-level change.

The GrIS SMB for the 35-year mean was  $123.7 \pm 253.4$  Gt yr<sup>-1</sup>, indicating a negative sea-level contribution, and  $-42.9 \pm 135.5$  Gt yr<sup>-1</sup> for 2005–2014, indicating a trend towards a less positive SMB value sea-level contribution (Table 1). This change in SMB between the two periods was mainly due to an increase in runoff of  $155.6 \pm 106.7$  Gt yr<sup>-1</sup>, where other water balance components showed relatively lesser increases. For comparison e.g., Vizcaino et al. (2013), Noël et al. (2016), and Wilton et al. (2016) have estimated the mean GrIS SMB to be  $359.3 \pm 120$  Gt yr<sup>-1</sup> (1960–2005),  $349.3$  Gt yr<sup>-1</sup> (1958–2015), and  $382 \pm 78$  Gt yr<sup>-1</sup> (1979–2012), respectively. For the GrIS, the 35-year mean SMB was negative for the northern regions, in balance for northeast Greenland, and positive for all other the southern regions and only positive for the southeastern, southwestern, and western sectors for 2005–2014

Formatted: Not Highlight

Formatted: Danish

Formatted: Not Highlight

(Table 1). Overall, the SMB patterns were highly controlled by the distribution of precipitation and runoff.

The linear trends for the different water balance components are shown in Table 1. For the 35-year period, only significant trends occurred for rain, surface melt, runoff, ablation, refreezing and retention, and SMB (highlighted in bold in Table 1), where all except SMB showed positive trends (note that SMB loss is calculated as negative by convention). In Figure 4, selected GrIS parameters are illustrated, where, for example, SMB showed a negative trend of -99.66.2 Gt decade<sup>-1</sup> (significant), heading towards a zero-less positive balance at the end of the simulation period. (Figure 4). For 2005–2014, however, the SMB trend was positive 24.216.6 Gt decade<sup>-1</sup> (insignificant). Similar positive SMB trends have previously been shown in studies by Hanna et al. (2011), Tedesco et al. (2014), Fettweis et al., (2008, 2011, 2013) and Wilton et al. (2016), even though variabilities in mean SMB occur between the different studies. Wilton et al. (2016) estimated the GrIS SMB to be ~100~150 Gt yr<sup>-1</sup> for 2002–2012 in the late 2000s and ~100 Gt for the years 2010–2012. Further, for 2005–2014, air temperature, precipitation, surface melt, sublimation and evaporation, and runoff trends were all negative (insignificant) (Figure 4 and Table 1).

Formatted: Not Highlight

Formatted: Not Highlight

#### 4.2 Greenland spatiotemporal runoff distribution and EOF analysis

The Greenland 35-year simulated catchment outlet runoff and specific runoff distribution are shown in Figure 5. Each circle represents the volume (individual catchment outlet hydrographs are not shown), including runoff from thousands of glaciers located between the GrIS margin and the surrounding seas. The 35-year mean catchment outlet runoff varied from <0.0001 to  $25.7\text{--}20 \times 10^9 \text{ m}^3$  (Figure 5a) and specific runoff from <0.1 to  $90427.5 \text{ L s}^{-1} \text{ km}^{-2}$

(Figure 5b). Catchment runoff variability depends on the regional climate conditions, land-ice area cover, elevation range (including hypsometry) within each catchment, and catchment area. Here the length in runoff season varied from two to three weeks in the north to four to six months in the south. The median annual catchment runoff and specific runoff were  $0.025\text{--}018 \times 10^9 \text{ m}^3$  and  $9\text{--}16.4 \text{ L s}^{-1} \text{ km}^{-2}$ , respectively. The median specific runoff value is in agreement with previous studies (e.g., Mernild et al. 2010a). Further, the variance in catchment runoff and specific runoff varied from  $<0.0001$  to  $87.3\text{--}1 \times 10^9 \text{ m}^3$  and  $<0.01$  to  $19.3\text{--}15.3 \text{ L s}^{-1} \text{ km}^{-2}$ , respectively, with a median variance of  $0.006\text{--}004 \times 10^9 \text{ m}^3$  and  $2.4\text{--}1.8 \text{ L s}^{-1} \text{ km}^{-2}$  (Figures 4a–5a and 4b–5b). Regarding the linear trend in annual runoff, both increasing and decreasing trends occurred over the 35 years. In total, 81 % (19 %) of all catchments had increasing (decreasing) runoff trends over the 35 years (all of the decreasing trends were insignificant). For western Greenland catchments, only increasing runoff trends occurred (Figures 5a and 4b–5b). The runoff and specific runoff trends varied among catchments from  $-0.09\text{--}06$  to  $5.43.8 \times 10^9 \text{ m}^3 \text{ decade}^{-1}$  and from  $-1.30.9$  to  $12.99.0 \text{ L s}^{-1} \text{ km}^{-2} \text{ decade}^{-1}$ , respectively, with a median value of  $\leq 0.001 \times 10^9 \text{ m}^3$  and  $0.5\text{--}4 \text{ L s}^{-1} \text{ km}^{-2} \text{ decade}^{-1}$  (Figures 4a–5a and 4b–5b).

The EOF analysis of runoff returned three axes that captured 25.26, 18.7 and 12.14 % of the ~~variation-variance~~ in runoff from the simulated SnowModel ERA-I annual catchment runoff (Figure 6a and S1). Following several significance tests, only EOF1 captured significant variation. In Figure 6a, the temporal pattern in EOF1, with a 5-year running mean, reveals a pattern of positive running mean values for the first two decades of the simulation period (1979–1999), and negative values hereafter (2000–2014). When EOF1 is positive, Greenland runoff is relatively low and vice versa (Figure 7b). Overall, this indicates a positive temporal trend in runoff; as EOF1 ~~goes down~~decreases, runoff ~~goes up~~increases. While not significant based on

Formatted: Not Highlight

Formatted: Not Highlight

Formatted: Not Highlight

Formatted: Not Highlight



EOF test metrics, EOF2 and EOF3 patterns are less pronounced and in anti-phase to each other (Figure [6S1](#)).

The temporal cycle of EOF patterns has associated spatial elements, derived from the eigenvectors (Figure [86c and S2](#)). The eigenvectors in Figures [8-6c and S2](#) reveal the spatial pattern as a correlation between temporal trends captured by the EOFs and each individual Greenland catchment. These data indicate that the temporal trend of increasing runoff captured in EOF1 is shared by nearly all catchments in Greenland ([Figure 6c](#)). Because decreasing EOF1 values indicate increasing runoff, a negative correlation with EOF1 in space indicates increasing runoff. Catchment numbers greater than #2500 (Figure [86c](#)) are located in Southeast Greenland and are in contrast to this. These catchments ([~20 % of the catchments in Southeast Greenland](#)) experience a distinct out-of-phase pattern of runoff compared to the [Southeast Greenland runoff and the](#) overall Greenland conditions for the last 35 years.

This difference between Southeast Greenland and the rest of Greenland supports previous findings (e.g., Lenaerts et al. 2015) proposing that variabilities in runoff are not only influenced by melt conditions, but also by precipitation patterns (primarily the end-of-winter snow accumulation), where high precipitation equals low runoff conditions such as in Southeast Greenland. Furthermore, patterns were also detected to be associated to EOF2 and EOF3 (Figures [8b and 8eS2](#)). These EOF2 and EOF3 patterns differed from EOF1, and they were associated with a different geographic breakdown, where both positive and negative correlations were seen for all regions. The physical mechanism behind these distributions is not clear.

There were ~~strong~~ correlations between the EOF1 and regional climate patterns expressed by the AMO and NAO (Figure [97](#)). We found a negative correlation between EOF1 and AMO ( $r = 0.68$ ; significant,  $p < 0.01$ ), suggesting that stronger AMO is associated with lower EOF1 values

577 which are indicative of higher runoff (Figure 9a7a). In contrast, we found a positive correlation  
578 between EOF1 and NAO ( $r = 0.40$ ; significant,  $p < 0.01$ ), suggesting that ~~stronger~~ NAO values  
579 are associated with higher EOF1 values which are indicative of lower runoff (Figure 79b).

580 ~~Additional insight into the time frame over which these correlations arises is seen in Figure 9.~~

581 For AMO, the lags are centered near zero, suggesting an immediate, real time correlation  
582 between AMO and runoff. In contrast, the strongest lag in the NAO-EOF1 relationships is at -2,  
583 suggesting a short delay in effects. Lags of 0 and -2 are not large, indicating that overall, large-  
584 scale natural variability in AMO and NAO are ~~closely~~ associated in time to catchment runoff  
585 variations in Greenland.

586 Mernild et al. (2011) emphasized that trends in AMO (smoothed) was analogous to trends  
587 in GrIS melt extent, where increasing AMO equaled increasing melt extent, and vice versa.  
588 Further, Chylek et al. (2010) showed that the Arctic detrended temperatures were highly  
589 correlated with AMO. However, this issue requires further investigation to establish the details  
590 of, and the mechanisms behind, the interrelationships.

## 591 5. Conclusions

592 Greenland catchment outlet runoff is rarely observed and studied, although quantification  
593 of runoff from Greenland is crucial for our understanding of the link between a changing climate  
594 and changes in the cryosphere, hydrosphere, and atmosphere. We have reconstructed the impact  
595 of changes in climate conditions on hydrological processes at the surface of the GrIS for the 35-  
596 year period 1979–2014. We have also simulated the Greenland spatiotemporal distribution of  
597 refreezing and retention, and freshwater runoff to surrounding seas by merging SnowModel (a  
598 spatially distributed meteorological, full surface energy balance, snow and ice evolution model)

600 with HydroFlow (a linear-reservoir run-off routing model) forced by ERA-I atmospheric forcing  
601 data. Before simulating the individual catchment runoff to downstream areas, the catchment  
602 divides and flow networks were estimated, yielding a total of 3,272 catchments in Greenland.

603 For the GrIS, the simulated spatial distribution and time series of surface hydrological  
604 processes were in accordance with previous studies, although precipitation and SMB were in the  
605 lower range of these studies. Overall, Greenland has warmed and the runoff from Greenland has  
606 increased in magnitude. Specifically, 81 % of the catchments showed increasing runoff trends  
607 over the simulation period, with relatively high and low mean catchment runoff from the  
608 southwestern and northern parts of Greenland, respectively. This indicates distinct regional-scale  
609 runoff variability in Greenland. Runoff variability with near zero lag time suggests a real-time  
610 covariation between the pattern in EOF1 and changes in AMO and NAO. This ~~indicates suggests~~  
611 that ~~runoff variations are related to~~ large-scale natural variability ~~of in~~-AMO and NAO ~~is closely~~  
612 ~~related to catchment runoff variations~~ in Greenland. The physical mechanism behind this  
613 phenomenon is unclear, unless it is a response to “long-term” cycles in AMO and NAO.

614 The simulated runoff can be used as boundary conditions in ocean models to understand  
615 hydrologic links between terrestrial and marine environments in the Arctic. Changes and  
616 variability in runoff from Greenland are expected to play an essential role in the hydrographic  
617 and circulation conditions in fjords and the surrounding ocean under a changing climate.

618

## 619 Acknowledgements

620 We thank the Nansen Environmental and Remote Sensing Center (NERSC) and Japan  
621 Society for the Promotion of Science (JSPS) for financial support under project number S17096,

Formatted: Indent: First line: 0.5"

622 and the Western Norway University of Applied Sciences (HVL) for travel funds. All model data  
623 requests should be addressed to the first author. The authors have no conflict of interest.

624  
625  
626  
627  
628  
629  
630  
631  
632  
633  
634  
635  
636  
637  
638  
639  
640  
641  
642  
643  
644  
645  
646  
647  
648  
649  
650  
651

## References

AMAP, 2017. Snow, Water, Ice and Permafrost. Summary for Policy-makers. Arctic Monitoring and Assessment Programme (AMAP), Oslo, Norway, 20 pp.

Bales, R. C., Guo, Q., Shen, D., McConnell, J. R., Du, G., Burkhart, J. F., Spikes, V. B., Hanna, E., and Cappelen, J. 2009. Annual accumulation for Greenland updated using ice core data developed during 2000–2006 and analysis, of daily coastal meteorological data. *J. Geophys. Res.*, 114, D06116, doi:10.1029/2008JD011208.

Bamber, J., van den Broeke, M., Ettema, J., Lenaerts, J., and Rignot, E., 2012. Recent large increases in freshwater fluxes from Greenland into the North Atlantic. *Geophys. Res. Letts.*, 39, L19501, doi:10.1029/2012GL052552.

Banwell, A., Hewitt, I., Willis, I., and Arnold, N. 2016. Moulin density controls drainage development beneath the Greenland ice sheet. *J. Geophys. Res. Earth Surf.*, 121, 2248–2269.

Bartholomew, I., Nienow, P., Mair, D., Hubbard, A., King, M. A., and Sole, A. 2010. Seasonal evolution of subglacial drainage and acceleration in a Greenland outlet glacier. *Nat. Geosci.*, 3(6), 408–411.

Bartholomew, I., Nienow, P., Sole, A., Mair, D., Cowton, T., and King, M. 2012. Short-term variability in Greenland ice sheet motion forces by time-varying meltwater drainage: Implications for the relationship between subglacial drainage system behavior and ice velocity. *J. Geophys. Res.*, 117, F03002, doi:10.1029/2011JF002220.

Beamer, J. P., Hill, D. F., Arendt, A., and Liston, G. E. 2016. High-resolution modeling of coastal freshwater discharge and glacier mass balance in the Gulf of Alaska watershed. *Water Resour. Res.*, 52, 3888–3909, doi:10.1002/2015WR018457.

Bliss, A., Hock, R., and Radić, V. 2014. Global response of glacier runoff to twenty-first century climate change. *J. Geophys. Res. Earth Surf.*, 119, doi:10.1002/2013JF002931.

683

684 Box, J. E. 2013. Greenland ice sheet mass balance reconstruction, Part II: Surface mass balance  
685 (1840–2010). *Journal of Climate*, 26, 6974–6989, doi:10.1175/JCLI-D-12-00518.1.

686

687 Box, J. E., Cappelen, J., Chen, C., Decker, D., Fettweis, X., Mote, T., Tedesco, M., van de Wal,  
688 R. S. W., and Wahr, J. 2012. Greenland Ice Sheet. In Jeffries, M. O., Richter-Menge, J. A., and  
689 Overland, J. E. (Eds). *Arctic Report Card 2012*, <http://www.arctic.noaa.gov/reportcard>.

690

691 Brown, J., Bradford, J., Harper, J., Pfeffer, W. T., Humphrey, N., and Mosley-Thompson, E.,  
692 2012. Georadar-derived estimates of firn density in the percolation zone, western Greenland ice  
693 sheet. *Journal of Geophysical Research*, 117, F01011, doi:10.1029/2011JF002089.

694

695 Carrivick, J. L., and Quincey, D. J., 2014. Progressive increase in number and volume of ice-  
696 marginal lakes on the western margin of the Greenland Ice Sheet. *Global and Planetary Change*,  
697 116, 156-163, doi:10.1016/j.gloplacha.2014.02.009.

698

699 Chen, X., Zhang, X., Church, J. A., Watson, C. S., King, M. A., Monselesan, D., Legresy, B.,  
700 and Harig C. 2017. The increasing rate of global mean sea-level rise during 1993–2014. *Nature*  
701 *Climate Change*, doi:10.1038/nclimate3325.

702

703 Chu, W., Creyts, T., and Bell, R. E., 2016. Rerouting of subglacial water flow between  
704 neighboring glaciers in West Greenland. *J. Geophys. Res. Earth Surf.*, 121, 925–938.

705

706 Church, J. A., Clark, P. U., Cazenave, A., Gregory, J. M., Jevrejeva, S., Levermann, A.,  
707 Merrifield, M. A., Milne, G. A., Nerem, R. S., Nunn, P. D., Payne, A. J., Pfeffer, W. T.,  
708 Stammer, D., and Unnikrishnan, A. S. 2013. Sea Level Change. In: *Climate Change 2013: The*  
709 *Physical Science Basis. Contribution of Working Group I to the Fifth Assessment Report of the*  
710 *Intergovernmental Panel on Climate Change* [Stocker, T.F., Qin, D., Plattner, G.-K., Tignor, M.,  
711 Allen, S.K., Boschung, J., Nauels, A., Xia, Y., Bex, V. and Midgley, P.M. (eds.)]. Cambridge  
712 University Press, Cambridge, United Kingdom and New York, NY, USA.

713

714 Chylek, P., C.K. Folland, G. Lesins and M.K. Dubey. 2010. Twentieth century bipolar seesaw of  
715 the Arctic and Antarctic surface air temperatures. *Geophys. Res. Lett.*, 37(8), L08703,  
716 doi:10.1029/2010GL042793.

717

718 Cuffey, K. M. and Paterson, W. S. B. 2010. *The Physics of Glaciers*. Fourth Edition. Elsevier,  
719 pp. 693.

720

721 Cullather R. I., Nowicki, S. M. J., Zhao, B., and Koenig, L. S. 2016. A Characterization of  
722 Greenland Ice Sheet Surface Melt and Runoff in Contemporary Reanalyses and a Regional  
723 Climate Model. *Front. Earth Sci.*, 4(10), doi:10.3389/feart.2016.00010.

724

725 Dee, D. P., Uppala, S. M., Simmons, A. J., Berrisford, P., Poli, P., Kobayashi, S., Andrae, U.,  
726 Balmaseda, M. A., Balsamo, G., Bauer, P., Bechtold, P., Beljaars, A. C. M., van de Berg, L.,  
727 Bidlot, J., Bormann, N., Delsol, C., Dragani, R., Fuentes, M., Geer, A. J., Haimberger, L., Healy,  
728 S. B., Hersbach, H., Holm, E. V., Isaksen, L., Kållberg, P., Kohler, M., Matricardi, M., McNally,  
729 A. P., Monge-Sanz, B. M., Morcrette, J.-J., Park, B.-K., Peubey, C., de Rosnay, P., Tavolato, C.,  
730 Thepaut, J.-N., Vitart, F. 2011. The ERA-Interim reanalysis: configuration and performance of  
731 the data assimilation system. *Q. J. R. Meteorol. Soc.*, 137, 553–597, doi:10.1002/qj.828.

732

733 Dickson, R. R., Osborn, T. J., Hurrell, J. W., Meincke, J., Blindheim, J., Adlandsvik, B., Vinje,  
734 T., Alekseev, G., and Maslowski, W. 2000. The Arctic Ocean response to the North Atlantic  
735 Oscillation. *Journal of Climate*, 13, 2671–2696.

736

737 Enderlin, E. M., Howat, I. M., Jeong, S., Hoh, M.-J., van Angelen, J. H., and van den Broeke, M.  
738 R. 2014. An improved mass budget for the Greenland ice sheet. *Geophysical Research Letters*,  
739 41(3), 866–872.

740

741 Ettema, J., van den Broeke, M. R., van Meijgaard, E., van den Berg, W. J., Bamber, J. L., Box, J.  
742 E., and Bales, R. C. 2009. Higher surface mass balance of the Greenland ice sheet revealed by  
743 high-resolution climate modeling. *Geophysical Research Letters*, 36, L12501.

744

745 Everett, A., Murray, T., Selmes, N., Rutt, I. C., Luckman, A., James, T. D., Clason, S., O'Leary,  
 746 M., Karunarathna, H., Moloney, V., and Reeve, D. E. 2016. Annual down-glacier drainage of  
 747 lakes and water-filled crevasses at Helheim Glacier, southeast Greenland. *J. Geophys. Res. Earth*  
 748 *Surf.*, 121, 1819–1833.  
 749  
 750 Fettweis, X., Box, J. E., Agosta, C., Amory, C., Kittel, C., Lang, C., van As, D., Machguth, H.,  
 751 and Gallée, H., 2017. Reconstructions of the 1900–2015 Greenland ice sheet surface mass  
 752 balance using the regional climate MAR model. *The Cryosphere*, 11, 1015–1033, doi:10.5194/tc-  
 753 11-1015-2017.  
 754  
 755 Fettweis, X., Franco, B., Tedesco, M., van Angelen, J. H., Lenaerts, J. T. M., van den Broeke, M.  
 756 R., and Gallée, H., 2013. Estimating the Greenland ice sheet surface mass balance contribution to  
 757 future sea level rise using the regional atmospheric climate model MAR. *The Cryosphere*, 7, 709  
 758 469–489.  
 759  
 760 Fettweis, X., Hanna, E., Gallée, H., Huybrechts, P., and Erpicum, M. 2008. Estimation of the  
 761 Greenland ice sheet surface mass balance for the 20th and 21st centuries, *The Cryosphere*, 2,  
 762 117–129, doi:10.5194/tc-2-117-2008.  
 763  
 764 Fettweis, X., Tedesco, M., van den Broeke, M., and Ettema, J., 2011. Melting trends over the  
 765 Greenland ice sheet (1958–2009) from spaceborne microwave data and regional climate models.  
 766 *The Cryosphere*, 5, 359–375.  
 767  
 768 Goodison, B. E., Sevruk, B., and Klemm, S. 1989. WMO solid precipitation measurement  
 769 intercomparison: objectives, methodology, analysis. IAHS publication, 179, 57–64.  
 770  
 771 Hanna, E., Fettweis, X., Mernild, S. H., Cappelen, J., Ribergaard, M., Shuman, C., Steffen, K.,  
 772 Wood, L., and Mote, T. 2014. Atmospheric and oceanic climate forcing of the exceptional  
 773 Greenland Ice Sheet surface melt in summer 2012. *International Journal of Climatology*, 34,  
 774 1022–1037.  
 775



776 Hanna, E., Huybrechts, P., Cappelen, J., Steffen, K., Bales, R., Burgess, E., McConnell, J.,  
 777 Steffensen, J. P., Van den Broeke, M., Wake, L., Bigg, B., Griffiths, M., and Savas, D. 2011.  
 778 Greenland Ice Sheet surface mass balance 1870 to 2010 based on Twentieth Century Reanalysis,  
 779 and links with global climate forcing, *Journal of Geophysical Research*, 116, D24121,  
 780 doi:10.1029/2011JD016387.  
 781  
 782 Hanna, E., Huybrechts, P., Steffen, K., Cappelen, J., Huff, R., Shuman, C., Irvine-Fynn, T.,  
 783 Wise, S., and Griffiths, M. 2008. Increased runoff from melt from the Greenland ice sheet: A  
 784 response to global warming. *Journal of Climate*, 21, 331–341.  
 785  
 786 Hanna, E., McConnell, J., Das, S., Cappelen, J., and Stephens, A. 2006. Observed and modelled  
 787 Greenland Ice Sheet snow accumulation, 1958–2003, and links with regional climate forcing.  
 788 *Journal of Climate*, 19(3), 344–358, doi:10.1175/JCLI3615.1.  
 789  
 790 Hanna, E., Navarro, F. J., Pattyn, F., Domingues, C., Fettweis, X., Ivins, E., Nicholls, R. J., Ritz,  
 791 C., Smith, B., Tulaczyk, S., Whitehouse, P., and Zwally, J. 2013. Ice-sheet mass balance and  
 792 climate change. *Nature*, 498, 51–59.  
 793  
 794 Hanna, E., Mernild, S. H., Cappelen, J., and Steffen, K. 2012. Recent warming in Greenland in a  
 795 long-term instrumental (1881–2012) climatic context. Part 1: Evaluation of surface air  
 796 temperature records. *Environmental Research Letters*, 7, 045404, doi:10.1088/1748-  
 797 9326/7/4/045404.  
 798  
 799 Haper, J., Humphrey, N., Pfeffer, W. T., Brown, J. and Fettweis, X. 2012. Greenland ice-sheet  
 800 contribution to sea-level rise buffered by meltwater storage in firn. *Nature*, 22117–22124.  
 801  
 802 Hasholt, B., Mikkelsen, A. B., Nielsen, H. M., and Larsen, M. A. D. 2013. Observations of  
 803 Runoff and Sediment and Dissolved Loads from the Greenland Ice Sheet at Kangerlussuaq, West  
 804 Greenland, 2007 to 2010. *Zeitschrift für Geomorphologie*, 57(2), 3–27, doi:10.1127/0372-  
 805 8854/2012/S-00121.  
 806

807 Hewitt, I. 2013. Seasonal changes in ice sheet motion due to melt water lubrication. *Earth Plant.*  
808 *Sci. Lett.*, 371–372, 16–25.

809

810 Hiemstra, C. A., Liston, G. E., and Reiners, W. A. 2006. Observing, modelling, and validating  
811 snow redistribution by wind in a Wyoming upper treeline landscape. *Ecol. Model.* 197, 35–51,  
812 doi: 10.1016/j.ecolmodel.2006.03.005.

813

814 ~~Howat, I. M., De la Peña, S., Van Angelen, J. H., Lenaerts, J. T. M., and Van den Broeke, M. R. 2013.~~  
815 ~~Expansion of meltwater lakes on the Greenland Ice Sheet. *The Cryosphere*, 7, 201–204.~~  
816 ~~doi:10.5194/te-7-201-2013.~~

817

818 Hurrell, J. W. 1995. Decadal trends in the North Atlantic Oscillation: regional temperatures and  
819 precipitation. *Science*, 269, 676–679. doi:10.1126/science.269.5224.676.

820

821 Hurrell, J. W. and van Loon, H. 1997. Decadal variations in climate associated with the North  
822 Atlantic oscillation, *Climate Change*, 36, 301–326.

823

824 Kaplan, A., Cane, M. A., Kushnir, Y. and Clement, A. C. 1998. Analyses of global sea surface  
825 temperatures 1856–1991. *Journal of Geophysical Research*, 103, 18575–18589.

826

827 Kobayashi, S., Ota, Y., Harada, Y., Ebata, A., Moriya, M., Onoda, H., Onogi, K., Kamahori, H.,  
828 Kobayashi, C., Endo, H., Miyaoka, K., and Takahashi, K. 2015. The JRA-55 Reanalysis:  
829 General Specifications and Basic Characteristics, *J. Meteorol. Soc. Jpn.*, 93, 5–48,  
830 doi:10.2151/jmsj.2015-001.

831

832 Kohler, T. J., Zarsky, J. D., Yde, J. C., Lamarche-Gagnon, G., Hawkings, J. R., Tedstone, A. J.,  
833 Wadham, J. L., Box, J. E., Beaton, A., and Stibal, M., 2017. Carbon dating reveals seasonal  
834 shifts in the source of sediments exported from the Greenland Ice Sheet. *Geophys. Res. Lett.*,  
835 44(12), 6209–6217.

836

Formatted: English (United States)

837 Koziol, C., Arnold, N., Pope, A., and Colgan, W., 2017. Quantifying supraglacial meltwater  
838 pathways in the Paakitsoq region, West Greenland. *J. Glaciol.*, 63(239), 464–476.  
839

840 Langen, P. L., Mottram, R. H., Christensen, J. H., Boberg, F., Rodehacke, C. B., Stendel, M., van  
841 As, D., Ahlstrøm, A. P., Mortensen, J., Rysgaard, S., Petersen, D., Svendsen, K. H.,  
842 Algeirsdottir, G. A., and Cappelen, J. 2015. Quantifying Energy and Mass Fluxes Controlling  
843 Godthåbsfjord Freshwater Input in a 5-km Simulation (1991–2012). *Journal of Climate*, 28,  
844 3694–3713, doi:10.1175/JCLI-D-14-00271.1.  
845

846 Lenaerts, J. T. M., Le Bars, D., van Kampenhout, L., Vizcaino, M., Enderlin, E. M., and van den  
847 Broeke, M. R. 2015. Representing Greenland ice sheet freshwater fluxes in climate models.  
848 *Geophys. Res. Lett.*, 42, 6373–6381, doi:10.1002/2015GL064738.  
849

850 Levinsen, J. F., Forsberg, R., Sørensen, L. S., and Khan, S. A. 2015. Essential Climate Variables  
851 for the Ice Sheets from Space and Airborne measurements. [Danmarks Tekniske Universitet](#)  
852 (DTU) PhD Thesis, Kgs. Lyngby, pp. 1–232.  
853

854 Lewis, S. M., and Smith, L. C. 2009. Hydrological drainage of the Greenland ice sheet. *Hydrol.*  
855 *Processes*, 23, 2004–2011, doi:10.1002/hyp.7343.  
856

857 Liston, G. E. 1995. Local advection of momentum, heat, and moisture during the melt of patchy  
858 snow covers. *J. Appl. Meteorol.*, 34, 1705–1715, doi:10.1175/1520-0450-34.7.1705.  
859

860 Liston, G. E. and Elder, K. 2006a. A distributed snow-evolution modeling system (SnowModel).  
861 *J. Hydrometeorol.*, 7, 1259–1276, doi:10.1175/JHM548.1.  
862

863 Liston, G. E. and Elder, K. 2006b. A meteorological distribution system for high-resolution  
864 terrestrial modeling (MicroMet). *J. Hydrometeorol.*, 7, 217–234, doi:10.1175/JHM486.1.  
865

Formatted: English (United Kingdom)

866 Liston, G. E., Haehnel, R. B., Sturm, M., Hiemstra, C. A., Berezovskaya, S., and Tabler, R. D.  
867 2007. Simulating complex snow distributions in windy environments using SnowTran-3D. J.  
868 Glaciol., 53, 241–256.

869

870 Liston, G. E. and Hiemstra, C. A. 2011. The changing cryosphere: pan-Arctic snow trends  
871 (1979–2009). J. Clim., 24, 5691–5712.

872

873 Liston, G. E. and Mernild, S. H. 2012. Greenland freshwater runoff. Part I: a runoff routing  
874 model for glaciated and non-glaciated landscapes (HydroFlow). J. Clim., 25(17), 5997–6014.

875

876 Liston, G. E. and Sturm, M. 1998. A snow-transport model for complex terrain. J. Glaciol., 44,  
877 498–516.

878

879 Liston, G. E. and Sturm, M. 2002. Winter precipitation patterns in Arctic Alaska determined from  
880 a blowing-snow model and snow depth observations. J. Hydrometeorol., 3, 646–659.

881

882 Liston, G. E., Winther, J.-G., Bruland, O., Elvehøy, H., and Sand, K. 1999. Below surface ice  
883 melt on the coastal Antarctic ice sheet. J. Glaciol., 45, 273–285.

884

885 Machguth, H., MacFerrin, M., van as, D., Box, J., Charalampidis, C., Colgan, W., Fausto, R. S.,  
886 Meijer, H. A. J., Mosley-Yhompson, E., and van de Wal, R. S. W. 2016. Greenland meltwater  
887 storage in firn limited by near-surface ice formation. Nature Climate Change, 6(4), 390–393,  
888 doi.org/10.1038/nclimate2899.

889

890 Mernild, S. H. 2016. Water balance from mountain glacier scale to ice sheet scale - With focus  
891 on Mittivakkat Gletscher, Southeast Greenland, and the Greenland Ice Sheet. Doctoral thesis.  
892 Faculty of Science, University of Copenhagen, Copenhagen, pp. 419.

893

894 Mernild, S. H., B. Hasholt and G. E. Liston 2006b. Water flow through Mittivakkat Glacier,  
895 Ammassalik Island, SE Greenland. Geografisk Tidsskrift-Danish Journal of Geography, 106(1),  
896 25–43.

Formatted: Font: (Default) Times New Roman, 12 pt

Formatted: Font: (Default) Times New Roman, 12 pt

897  
898 Mernild, S. H., Hanna, E., McConnell, J. R., Sigl, M., Beckerman, A. P., Yde, J. C., Cappelen, J.,  
899 and Steffen, K. 2015. Greenland precipitation trends in a long-term instrumental climate context  
900 (1890–2012): Evaluation of coastal and ice core records. *International Journal of Climatology*,  
901 35, 303–320, doi:10.1002/joc.3986.  
902  
903 Mernild, S. H. and Liston, G. E. 2010. The influence of air temperature inversion on snow melt  
904 and glacier surface mass-balance simulations, SW Ammassalik Island, SE Greenland. *Journal of*  
905 *Applied Meteorology and Climate*, 49(1), 47–67.  
906  
907 Mernild, S. H. and Liston, G. E. 2012. Greenland freshwater runoff. Part II: distribution and  
908 trends, 1960–2010. *J. Clim.*, 25(17), 6015–6035.  
909  
910 Mernild, S. H., Liston, G. E., Hasholt, B., and Knudsen, N. T. 2006a. Snow distribution and melt  
911 modeling for Mittivakkat Glacier, Ammassalik Island, SE Greenland. *Journal of*  
912 *Hydrometeorology*, 7, 808–824.  
913  
914 Mernild, S. H., and Liston, G. E., and Hiemstra, C. A. 2014. Northern hemisphere glaciers and  
915 ice caps surface mass balance and contribution to sea-level rise. *J. Clim.*, 27(15), 6051–6073,  
916 doi:10.1175/JCLI-D-13-00669.1.  
917  
918 Mernild, S. H., Liston, G. E., Hiemstra, C. A. and Christensen, J. H. 2010<sup>a</sup>. Greenland Ice Sheet  
919 surface mass-balance modeling in a 131 year perspective 1950–2080. *Journal of*  
920 *Hydrometeorology*, 11(1), 3–25, doi.org/10.1175/2009JHM1140.1.  
921  
922 Mernild, S. H., Liston, G. E., Hiemstra, C. A., and Steffen, K. 2008. Surface Melt Area and  
923 Water Balance Modeling on the Greenland Ice Sheet 1995–2005. *Journal of Hydrometeorology*,  
924 9(6), 1191–1211, doi.org/10.1175/2008JHM957.1.  
925  
926 Mernild, S. H., Liston, G. E., van As, D., Hasholt, B., and Yde, J. C. 2018<sup>7</sup>. High-resolution ice  
927 sheet surface mass-balance and spatiotemporal runoff simulations: Kangerlussuaq, West

928 Greenland. ~~Accepted~~ Arctic, Antarctic, and Alpine Research (~~Special Issue, Kangerlussuaq~~).  
929 [doi.org/10.1080/15230430.2017.1415856](https://doi.org/10.1080/15230430.2017.1415856).

Formatted: Font: (Default) Times New Roman, 12 pt

931 Mernild, S. H., Mote, T., and Liston, G. E. 2011. Greenland Ice Sheet surface melt extent and  
932 trends, 1960–2010. *Journal of Glaciology*, 57(204), 621–628.

933  
934 Mernild, S. H., Liston, G. E., Hiemstra, C. A., Wilson, R. 2017. The Andes Cordillera. Part III:  
935 Glacier Surface Mass Balance and Contribution to Sea Level Rise (1979–2014). *International*  
936 *Journal of Climatology*, 37(7), 3154–3174, doi: 10.1002/joc.4907.

Formatted: Font: Times New Roman

Formatted: Line spacing: 1.5 lines

Formatted: Font: Times New Roman, Not Bold, Not Italic

Formatted: Font: Times New Roman

Formatted: Default Paragraph Font, Font: Times New Roman, Font color: Custom Color(54,31,14))

Formatted: Font: Times New Roman

Formatted: Font: 12 pt

938 Metcalfe, J. R., Ishida, S., and Goodison, B. E. 1994. A corrected precipitation archive for the  
939 Northwest Territories of Canada,  
940 [http://www.usask.ca/geography/MAGS/Data/Public\\_Data/precip\\_corr/pcpncor\\_e.htm](http://www.usask.ca/geography/MAGS/Data/Public_Data/precip_corr/pcpncor_e.htm).

941  
942 Nghiem, S. V., Hall, D. K., Mote, T. L., Tedesco, M., Albert, M. R., Keegann, K., Shuman, C.  
943 A., DiGirolamo, N. E., and Neumann, G. 2012. The extreme melt across the Greenland ice sheet  
944 in 2012. *Geophysical Research Letters*, 39, L20502.

945  
946 Nick, F. M., Vieli, A., Howat, I. M., and Joughin, I. R. 2009. Large-scale changes in Greenland  
947 outlet glacier dynamics triggered at the terminus. *Nature Geoscience*, 2(2), 110–114,  
948 doi:10.1038/ngeo394.

949  
950 Noël, B., van de Berg, W. L., Lhermitte, S., Wouters; B., Machguth, H., Howat, I., Citterio, M.,  
951 Moholdt, G., Lenaerts, J. T. M., and van den Broeke, M. R. 2017. A tipping point in refreezing  
952 accelerates mass loss of Greenland's glaciers and ice caps. *Nature Communications*, 8, 1–8,  
953 doi:10.1038/ncomms14730.

954  
955 Noël, B., van de Berg, W. J., Machguth, H., Lhermitte, S., Howat, I., Fettweis, X., and van den  
956 Broeke, M. R. 2016. A daily 1 km resolution data set of down scaled Greenland ice sheet  
957 surface mass balance (1958–2015). *The Cryosphere*, 10, 2361–2377, doi:10.5194/tc-10-2361-  
958 2016.

Formatted: English (United Kingdom)

Formatted: English (United States)

Formatted: English (United States)

Formatted: English (United States)

Formatted: English (United States)

Formatted: English (United States)

Formatted: English (United States)

Formatted: English (United States)

Formatted: English (United States)

Formatted: English (United States)

959

960 Overland, J. E., Francis, J., Hanna, E. and Wang, M. 2012. The recent shift in early summer  
 961 arctic atmospheric circulation. *Geophysical Research Letters*, 39, L19804.

962

963 Preisendorfer, R.W. 1998. Principal Component Analysis in Meteorology and Oceanography. In:  
 964 Mobley, C.D. (Ed.) Elsevier, Amsterdam, p. 452.

965

966 Rahmstorf, S., and Coauthors. 2005. Thermohaline circulation hysteresis: A model  
 967 intercomparison. *Geophys. Res. Lett.*, 32, L23605, doi:10.1029/2005GL023655.

968

969 Rasmussen, R., Baker, B., Kochendorfer, J., Meyers, T., Landolt, S., Fischer, A. P., Black, J.,  
 970 Theriault, J. M., Kucera, p., Gochis, D., Smith, C., Nitu, R., Hall, M., Ikeda, K., and Gutmann,  
 971 E. 2012. How well are we measuring snow? The NOAA/FAA/NCAR Winter Precipitation Test  
 972 Bed. *BAMS*, 811–829.

973

974 Rignot, E. and Mouginot, J. 2012. Ice flow in Greenland for the International Polar Year 2008–  
 975 2009. *Geophysical Research Letters*, 39, L11501, doi:10.1029/2012GL051634.

976

977 Rignot, E., Velicogna, I., van den Broeke, M. R., Monaghan, A., and Lenaerts, J. 2011.  
 978 Acceleration of the contribution of the Greenland and Antarctic ice sheets to sea level rise.  
 979 *Geophysical Research Letters*, 38, L05503.

980

981 Roberts, M.J. 2005. Jökulhlaups: a reassessment of floodwater flow through glaciers. *Rev.*  
 982 *Geophys.*, 43(1), RG1002, doi:10.1029/2003RG000147.

983

984 Rogers, A. N., Bromwich, D. H., Sinclair, E. N. and Cullather, R. I., 2001. The atmospheric  
 985 hydrological cycle over the Arctic basins from reanalysis. Part II: Inter-annual variability.  
 986 *Journal of Climate*, 14, 2414–2429.

987

988 Selmes, N., Murray, T., and James, T. D. 2011. Fast draining lakes on the Greenland ice sheet.  
 989 *Geophys Res. Lett.*, 38(15), doi:10.1029/2011GL047872.

990  
 991 Shepherd, A. et al. 2012. A Reconciled Estimate of Ice-Sheet Mass Balance. *Science*, 338,  
 992 1183–1189.  
 993  
 994 Sparnocchia S, Pinardi N, and Demirov E. 2003. Multivariate empirical orthogonal function  
 995 analysis of the upper thermocline structure of the Mediterranean Sea from observations and  
 996 model simulations. *Ann. Geophys*, 21, 167–187.  
 997  
 998 Sugden, D.E., Clapperton, C. M, and Knight, P. G.1985. A jökulhlaup near Søndre Strømfjord,  
 999 West Greenland, and some effects on the ice-sheet margin. *Journal of Glaciology*, 31(109), 366–  
 1000 368.  
 1001  
 1002 Steger, C. R., Reijmer, C. H., van den Broeke, M. R., Wever, N., Forster, R. R., Koenig, L. S.,  
 1003 Kuipers Munneke, P., Lehning, M., Lhermitte, S., Ligtenberg, S. R. M., Miège, C., and Noël, B.  
 1004 P., Y., 2017, Firn Meltwater Retention on the Greenland Ice Sheet: A Model Comparison. *Front.*  
 1005 *Earth Sci.*, 5:3. doi: 10.3389/feart.2017.00003.  
 1006  
 1007 Steffen, K. 1995. Surface energy exchange at the equilibrium line on the Greenland ice sheet  
 1008 during onset of melt. *Annals of Glaciology*, 21, 13–18.  
 1009  
 1010 Straneo, F., Curry, R. G., Sutherland, D. A., Hamilton, G. S., Cenedese, C., Våge, K., and Sterns,  
 1011 L. A. 2011. Impact of fjord dynamics and glacial runoff on the circulation near Helheim Glacier.  
 1012 *Nat. Geosci.*, 4, 322–327, doi:10.1038/ngeo1109.  
 1013  
 1014 Tedesco, M., Willis, I. C., Hoffman, M. J., Banwell, A. F., Alexander, P., and Arnold, N. S.  
 1015 2013. Ice dynamic response to two modes of surface lake drainage on the Greenland ice sheet.  
 1016 *Environ. Res. Lett.*, 8(3), 34007, doi:10.1088/1748-9326/8/3/034007.  
 1017  
 1018 Tedesco, M., Box, J. E., Cappelen, J., Fettweis, X., Mote, T., van de Wal, R. S. W., Smeets, C. J.  
 1019 P. P., and Wahr, J. 2014. Greenland Ice Sheet. In Jeffries, M. O., Richter-Menge, J. A., and  
 1020 Overland, J. E. (eds.). *Arctic Report Card 2014*.

Formatted



1021

1022 Tedesco, M., Box, J. E., Cappelen, J., Fausto, R. S., Fettweis, X., Mote, T., Smeets C. J. P. P.,

1023 van As, D., Velicogna, I., van de Wal, R. S. W. and Wahr, J. 2016. Greenland Ice Sheet. In

1024 Richter-Menge, J. A., Overland, J. E., and Mathis, J. T. (eds.). Arctic Card Report 2016.

1025

1026 Uppala, S. M., Kållberg, P. W., Simmons, A. J., Andrae, U., Da Costa Bechtold, V., Fiorino, M.,

1027 Gibson, J.K., Haseler, J., Hernandez, A., Kelly, G. A., Li, X., Onogi, K., Saarinen, S., Sokka,

1028 N., Allan, R. P., Anderson, E., Arpe, K., Balmaseda, M. A., Beljaars, A. C. M., Van De Berg, L.,

1029 Bidlot, J., Bormann, N., Caires, S., Chevallier, F., Dethof, A., Dragosavac, M., Fisher, M.,

1030 Fuentes, M., Hagemann, S., Hólm, E., Hoskins, B. J., Isaksen, L., Janssen, P. A. E. M., Jenne, R.,

1031 McNally, A. P., Mahfouf, J.-F., Morcrette, J.-J., Rayner, N. A., Saunders, R.W., Simon, P., Sterl,

1032 A., Trenbreth, K. E., Untch, A., Vasiljevic, D., Viterbo, P., and Woollen, J.: The ERA-40 re-

1033 analysis, Q. J. Roy. Meteor. Soc., 131, 2961–3012, doi:10.1256/qj.04.176, 2005.

1034

1035 van Angelen, J. H., Lenaerts, J. T. M., van den Broeke, J. T. M., Fettweis, X., van Meijgaard, E.

1036 2013. Rapid loss of firn pore space accelerates 21 century Greenland mass loss. Geophysical

1037 Research Letter, 40, 2109–2113.

1038

1039 van As., D, Box, J. E., and Fausto, R. S., 2016: Challenges of Quantifying Meltwater Retention

1040 in Snow and Firn: An Expert Elicitation. *Frontiers in Earth Science*, 4(101), 1–5.

1041

1042 van As, D. Hasholt, B., Ahlstrøm, A. P., Box, J. E., Cappelen, J., Colgan, W., Fausto, R. S.,

1043 Mernild, S. H., Mikkelsen, A .B., Noël, B. P.Y., Petersen, D., and Van den Broeke, M. R. 2018.

1044 The longest observationally-constrained record of Greenland ice sheet meltwater discharge

1045 (1949–2016). Accepted, Arctic, Antarctic, and Alpine Research (Special Issue).

1046

1047 van den Broeke, M. R., Enderlin, E. M., Howat, I. M., Munneke, P.K., Noël, B. P., Y., van de

1048 Berg, W. J., van Meijgaard, E., and Wouters, B. 2016. On the recent contribution of the

1049 Greenland ice sheet to sea level change. The Cryosphere, 10, 1933–1946, doi:10.5194/tc-10-

1050 1933-2016.

1051

**Formatted:** Font: Not Bold

**Formatted:** Font: (Default) Times New Roman, 12 pt, Not Highlight

**Formatted:** Font: (Default) Times New Roman, 12 pt

**Formatted:** No Spacing, Line spacing: 1.5 lines

**Formatted:** Font: (Default) Times New Roman, 12 pt

**Formatted:** Font: (Default) Times New Roman, 12 pt, Not Bold, Not Italic

**Formatted:** Font: 12 pt

**Formatted:** Norwegian (Bokmål)

**Formatted:** English (United States)

**Formatted:** English (United States)

**Formatted:** English (United States)

**Formatted:** English (United States)

**Formatted:** Font: Not Bold

1052 van den Broeke, M., Smeets, P., Ettema, J., and Munneke, P. K. 2008a. Surface radiation balance  
1053 in the ablation zone of the west Greenland ice sheet, *J. Geophys. Res.*, 113, D13105,  
1054 doi:10.1029/2007/JD009283.

Formatted: English (United Kingdom)

1055  
1056 van den Broeke, M., Smeets, P., Ettema, J., van der Veen, C., van de Wal, R., and Oerlemans, J.  
1057 2008b. Partitioning of melt energy and meltwater fluxes in the ablation zone of the west  
1058 Greenland ice sheet, *The Cryosphere*, 2, 179–189, doi:10.5194/tc-2-179-2008.

1059  
1060  
1061 van de Wal, R. S. W., Greuell, W., van den Broeke, M. R., Reijmer, C. H., and Oerlemans, J.  
1062 2005. Surface mass-balance observations and automatic weather station data along a transect  
1063 near Kangerlussuaq, West Greenland, *Ann. Glaciol.*, 42, 311–316.

Formatted: Norwegian (Bokmål)

1064  
1065 van de Wal, R. S. W., Boot, W., van den Broeke, M., Smeets, C. J. P. P., Reijmer, C. H., Donker,  
1066 J. J. A., and Oerlemans, J. 2008. Large and rapid melt-induced velocity changes in the ablation  
1067 zone of the Greenland ice sheet. *Science*, 321, 111–113.

1068  
1069 van der Veen, C. J. 2007. Fracture propagation as a means of rapidly transferring surface  
1070 meltwater to the base of glaciers. *Geophys. Res. Lett.*, 34, L01501.

1071  
1072 Weijer, W., M. E. Maltrud, M. W. Hecht, H. A. Dijkstra, and M. A. Kliphuis, 2012. Response of  
1073 the Atlantic Ocean circulation to Greenland Ice Sheet melting in a strongly-eddy ocean  
1074 model. *Geophys. Res. Lett.*, 39, L09606, doi:10.1029/2012GL051611.

1075  
1076 Wilton, D. J., Jowett, A., Hanna, E., Bigg, G. R., van den Broeke, M. R., Fettweis, X., and  
1077 Huybrechts, P., 2017. High resolution (1 km) positive degree-day modelling of Greenland ice  
1078 sheet surface mass balance, 1870-2012 using reanalysis data. *Journal of Glaciology*, 63(237),  
1079 176–193.

1080  
1081 Vizcaino, M., Lipscomb, W. H., Sacks, W. J., van Angelen, J. H., Wouters, B., and van den  
1082 Broeke, M. R. 2013. Greenland Surface Mass Balance as Simulated by the Community Earth

Formatted: Font: (Default) Times New Roman, 12 pt, Not Bold

1083 [System Model. Part I: Model Evaluation and 1850-2005 Results. Journal of Climate, 26, 7793–](#)  
1084 [7812, doi.10.1175/JCLI-D-12-00615.1.](#)  
1085  
1086 Yang, D., Ishida, S., Goodison, B. E., and Gunter, T. 1999. Bias correction of daily precipitation  
1087 measurements for Greenland. J. Geophys. Res. 104(D6), 6171–6181,  
1088 doi:10.1029/1998JD200110.  
1089  
1090 Zwally, H. J., Abdalati, W., Herring, T., Larson, K., Saba, J., and Steffen, K. 2002. Surface melt-  
1091 induced acceleration of Greenland ice-sheet flow. Science, 297, 218–222.  
1092  
1093  
1094  
1095  
1096  
1097  
1098  
1099  
1100  
1101  
1102  
1103  
1104  
1105

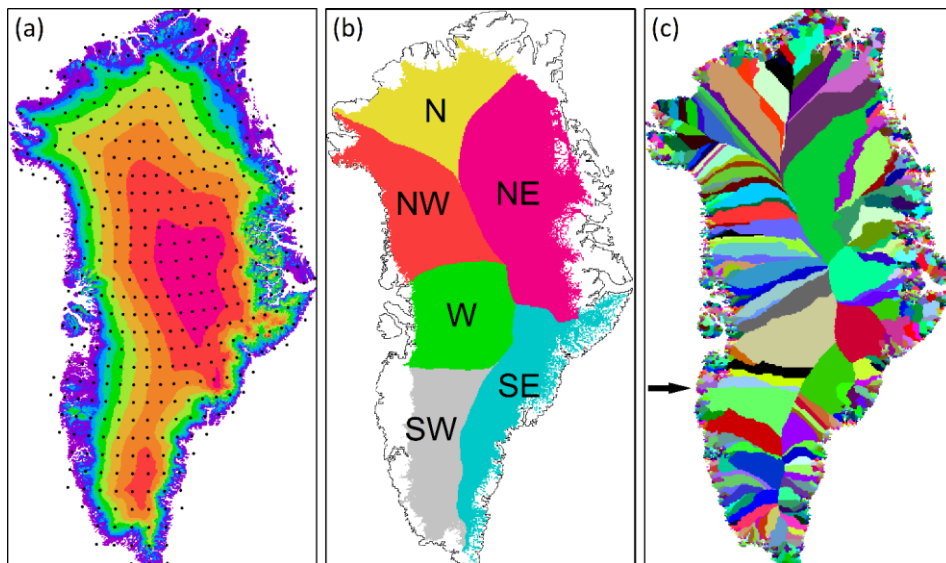


**Figure 1:** (a) Greenland simulation domain with topography (500-m contour interval) and locations of ERA-I atmospheric forcing grid points used in the model simulations (black dots; to improve clarity only every other grid point was plotted in x and y, i.e., 25 % of the grid points used are shown); (b) the major regional division of the GrIS following Rignot et al. (unpublished); and (c) HydroFlow simulated individual Greenland drainage catchments ( $n = 3,272$ ; represented by multiple colors). The approximate location of the Kangerlussuaq catchment is shown with a black arrow [from where the SnowModel evaluations were conducted.](#)

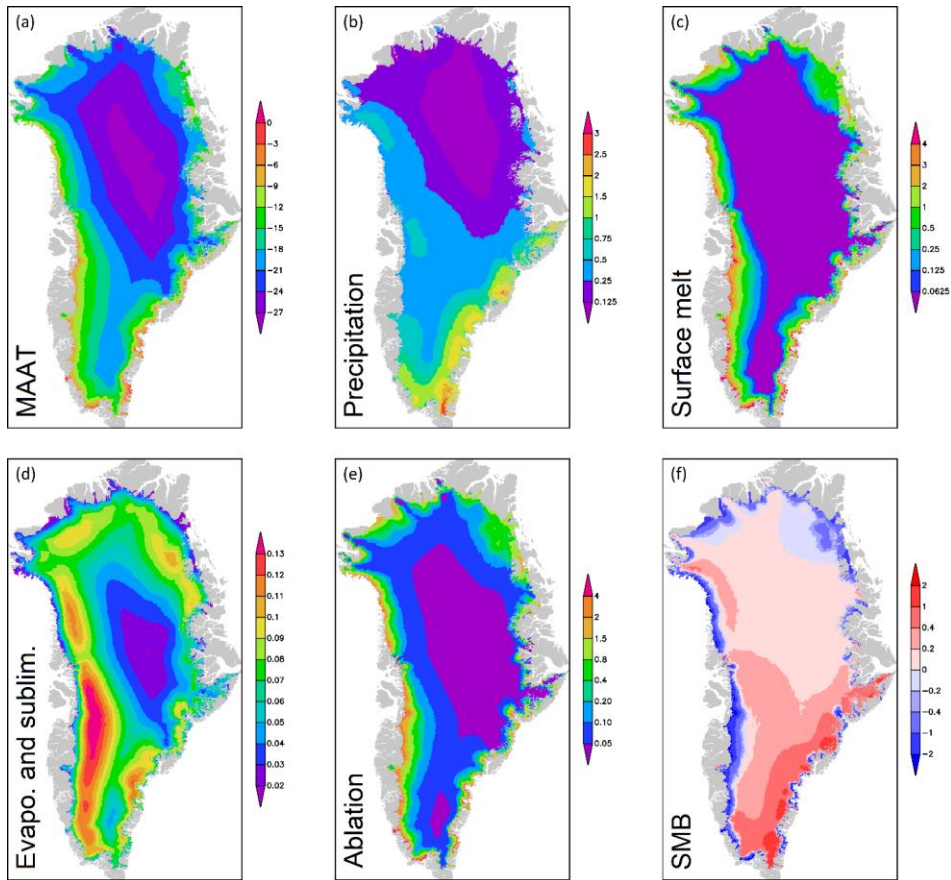
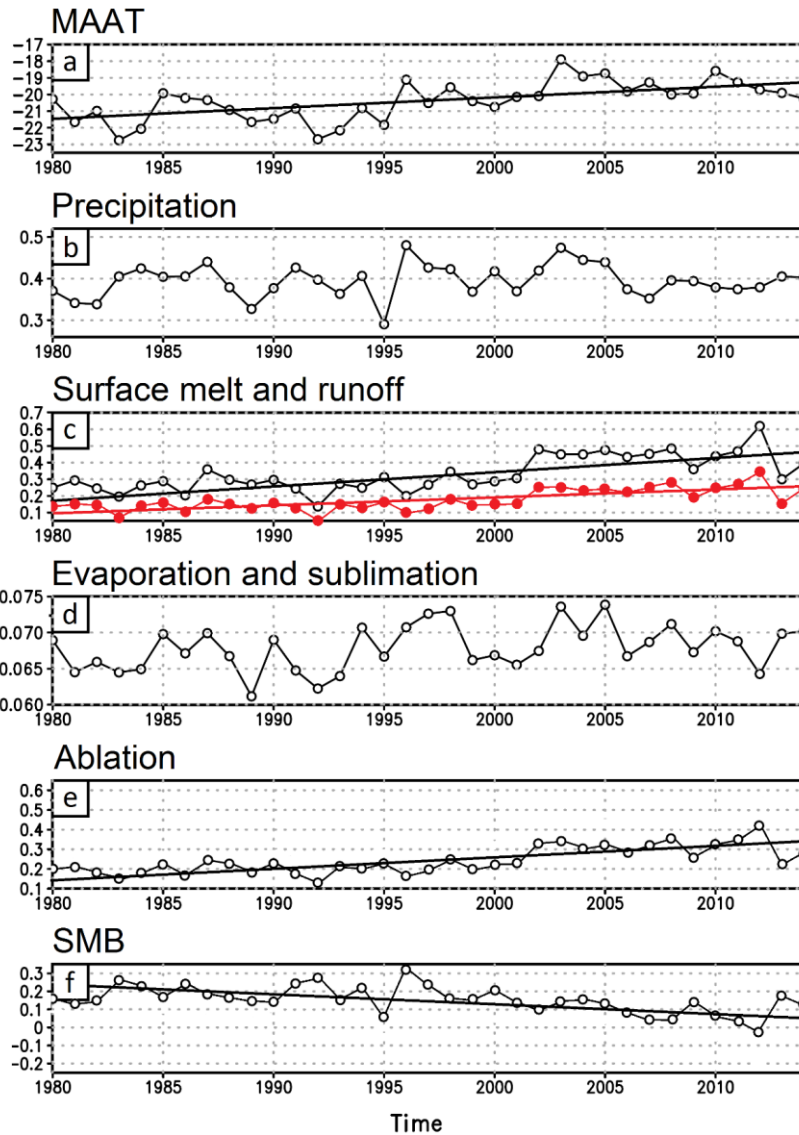


**Figure 2:** SnowModel ERA-I simulated 35-year mean spatial GrIS surface (1979–2014): (a) MAAT (°C); (b) precipitation (m w.e.); (c) surface melt (snow and ice melt) (m w.e.); (d) evaporation and sublimation (m w.e.); (e) ablation (m w.e.); and (f) SMB (m w.e.).

Formatted: Not Highlight





1140

1141 **Figure 4:** SnowModel ERA-I simulated time series of GrIS annual mean (1979–2014): (a)

1142 MAAT (°C); (b) precipitation (m w.e.); (c) surface melt (snow and ice melt) ~~(m w.e.)~~and runoff

1143 (red time series) (m w.e.); (d) evaporation and sublimation (m w.e.); (e) ablation (m w.e.); and (f)

1144 SMB (m w.e.). Only significant linear trends are shown.

Formatted: Not Highlight

Formatted: Not Highlight

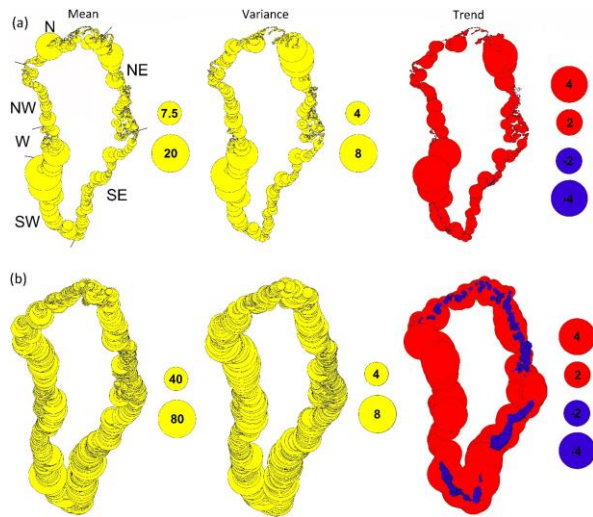


**Figure 5:** SnowModel ERA-I simulated 35-year spatial Greenland catchment runoff (1979–2014): (a) mean runoff ( $\times 10^9 \text{ m}^3$ ) (the locations of the major regions SW, W, NW, etc., are illustrated), runoff variance (here illustrated as one standard deviation;  $\times 10^9 \text{ m}^3$ ), and decadal runoff trends (linear;  $\times 10^9 \text{ m}^3 \text{ decade}^{-1}$ ) (catchments with increasing runoff trends are shown with red and decreasing trends with blue colors); and (b) mean specific runoff ( $\text{L s}^{-1} \text{ km}^2$ ), specific runoff variance ( $\text{L s}^{-1} \text{ km}^2$ ), and specific runoff trends (linear;  $\text{L s}^{-1} \text{ km}^2 \text{ decade}^{-1}$ ).

Formatted: Not Highlight



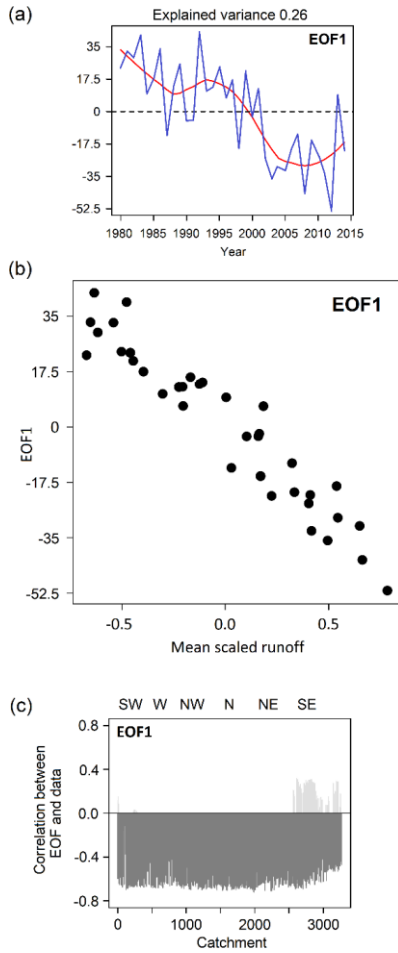


**Figure 6:** (a) SnowModel ERA-I simulated runoff time series (1979–2014) of the empirical orthogonal functions (black curve) and 5-year running mean smoothing line (red curve) of EOF1 (significant); (b) EOF1 cross correlation relationships with mean annual scaled runoff from Greenland; and (c) Eigenvector correlation values for each simulated catchment (1 to 3,272) for EOF1. From left to right on the lower x-axis the catchments follows the clockwise path from the southern tip of Greenland (Southwest Greenland, Catchment 1) to the northern part (N section) and back to the southern tip (Southeast Greenland, Catchment 3,272). The location of the major regions: SW, W, NW, etc., are shown on the upper x-axis.

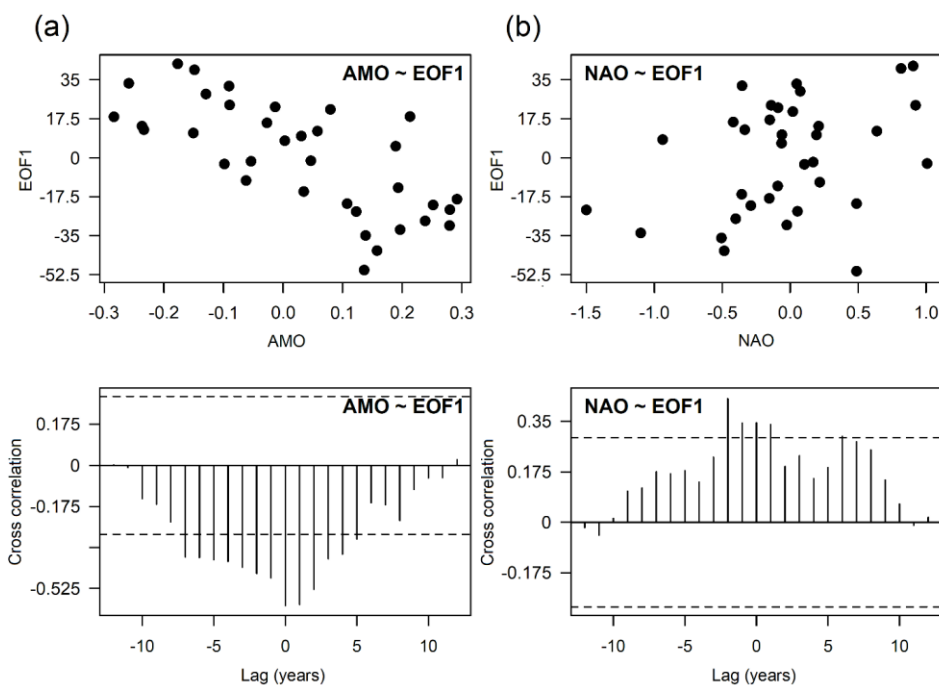


**Figure 7:** EOF1 cross correlation relationships between simulated Greenland runoff: (a) AMO and (b) NAO. The horizontal dashed lines on each of the column charts indicate the significance (95% confidence).

**Table 1:** Regional breakdown of GrIS surface mean annual conditions (units are in Gt) and trends (linear; Gt decade<sup>-1</sup>): precipitation (P) (including rain and snow), surface melt, evaporation (E) and sublimation (Su), runoff (R), ablation, refreezing and retention (rain and surface melt minus runoff), and surface mass-balance (SMB) for GrIS and for each of the six regions both from 1979–2014 (35 years) and 2005–2014 (10 years). Specifically for rain the %-value of total precipitation is shown. Trends are shown in paragraphs for the GrIS column. Significant trends ( $p < 0.05$ ) are highlighted in bold.

	N (229,075 km <sup>2</sup> )	NE (454,900 km <sup>2</sup> )	SE (250,425 km <sup>2</sup> )	SW (213,550 km <sup>2</sup> )	W (231,150 km <sup>2</sup> )	NW (267,075 km <sup>2</sup> )	GrIS (1,646,175 km <sup>2</sup> )
1979–2014							
P	31.1 ± 5.4	68.4 ± 10.6	242.6 ± 39.1	142.3 ± 23.3	85.4 ± 13.5	84.2 ± 13.9	653.9 ± 66.4 (9.0)
P (rain)	0.4 ± 0.2 (1 %)	0.4 ± 0.2 (<1 %)	4.2 ± 1.8 (2 %)	6.6 ± 2.8 (5 %)	1.7 ± 0.8 (2 %)	2.2 ± 1.1 (3 %)	15.3 ± 5.4 (2 %) <b>(3.0)</b>
P (snow)	30.7 ± 5.3	68.0 ± 10.5	238.5 ± 38.7	135.7 ± 22.7	83.7 ± 13.2	82.0 ± 13.5	638.6 ± 65.0 (6.0)
Surface melt	57.2 ± 24.1	72.2 ± 33.8	101.0 ± 27.1	155.2 ± 48.4	67.4 ± 24.0	89.8 ± 33.2	542.9 ± 175.3 <b>(121.7)</b>
E + Su	15.7 ± 0.9	25.3 ± 1.6	16.8 ± 0.8	20.3 ± 1.7	16.4 ± 1.1	17.7 ± 0.9	112.2 ± 5.2 (1.8)
R	34.5 ± 15.7	43.3 ± 21.8	47.8 ± 14.5	77.7 ± 28.9	37.0 ± 13.4	48.4 ± 19.4	288.7 ± 104.3 <b>(73.4)</b>
Ablation (E + Su + R)	50.2 ± 15.6	68.5 ± 21.8	64.6 ± 14.9	98.1 ± 29.2	54.4 ± 13.9	66.0 ± 19.8	400.9 ± 106.2 <b>(75.2)</b>
Refreezing and retention	23.1 ± 8.7 (40 %)	29.4 ± 12.5 (41 %)	57.5 ± 14.5 (57 %)	84.1 ± 23.2 (54 %)	32.1 ± 11.4 (46 %)	43.7 ± 14.9 (48 %)	269.9 ± 77.4 (49 %) <b>(51.3)</b>
SMB	-19.2 ± 17.9	-0.2 ± 23.3	178.1 ± 41.7	44.3 ± 39.2	32.1 ± 18.9	18.2 ± 24.4	253.4 ± 121.4 <b>(-66.2)</b>
2005–2014							
P	30.9 ± 5.1	71.0 ± 11.9	232.4 ± 25.2	138.5 ± 16.1	86.4 ± 8.6	85.3 ± 16.9	645.0 ± 39.0 (-5.1)
P (rain)	0.5 ± 0.3 (2 %)	0.4 ± 0.2 (<1 %)	5.2 ± 1.9 (2 %)	7.8 ± 2.3 (6 %)	2.0 ± 0.6 (2 %)	2.9 ± 1.3 (4 %)	18.7 ± 3.4 (3 %) (-2.8)
P (snow)	30.4 ± 5.0	70.6 ± 11.9	227.1 ± 25.0	130.8 ± 15.7	84.4 ± 8.6	82.9 ± 16.4	626.3 ± 39.2 (-2.3)
Surface melt	75.9 ± 26.9	101.7 ± 34.5	129.7 ± 16.3	202.4 ± 39.2	89.3 ± 19.7	124.6 ± 26.8	713.4 ± 138.6 (-79.7)
E + Su	15.7 ± 1.0	25.9 ± 1.1	17.3 ± 0.9	20.7 ± 1.5	16.7 ± 0.8	17.8 ± 0.9	114.1 ± 4.3 (-3.8)
R	46.6 ± 17.3	61.7 ± 21.4	63.3 ± 10.0	106.6 ± 25.0	49.1 ± 10.5	68.7 ± 15.5	395.4 ± 82.7 (-26.0)
Ablation (E + Su + R)	62.3 ± 17.0	87.6 ± 21.2	80.6 ± 9.7	127.3 ± 23.9	65.9 ± 10.2	86.5 ± 15.6	510.0 ± 81.7 (-17.9)
Refreezing and retention	29.7 ± 10.0 (39 %)	40.5 ± 13.6 (40 %)	66.4 ± 8.7 (51 %)	95.8 ± 18.5 (47 %)	40.2 ± 9.9 (45 %)	55.9 ± 13.0 (45 %)	318.0 ± 62.8 (45 %) (-64.6)
SMB	-31.4 ± 18.7	-16.5 ± 22.0	151.8 ± 32.0	11.3 ± 34.5	20.6 ± 12.6	-0.7 ± 24.3	135.5 ± 98.2 (16.6)

1194

1195

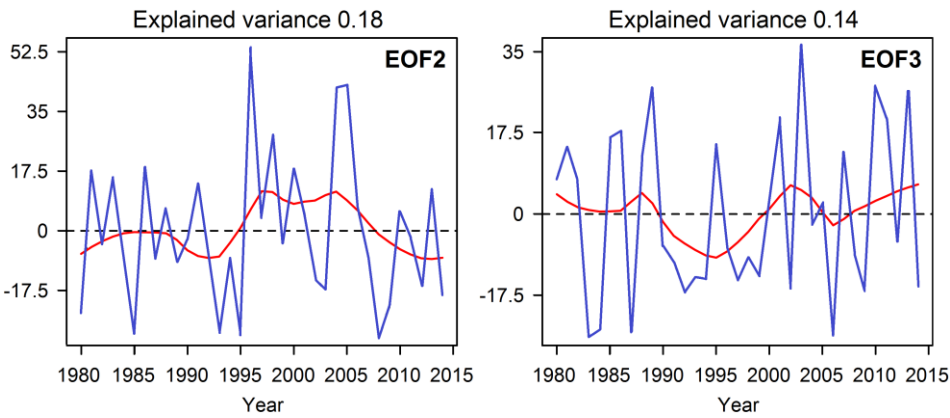
1196 **Table 2:** Regional breakdown of GrIS specific runoff ( $\text{L s}^{-1} \text{ km}^{-2}$ ) for GrIS and each of the six  
1197 individual sections both from 1979–2014 and 2005–2014.

1198

	N	NE	SE	SW	W	NW	GrIS
1979–2014	4.8	3.0	6.0	11.5	5.1	5.7	5.6
2005–2014	6.5	4.3	8.0	15.8	6.7	8.2	7.6

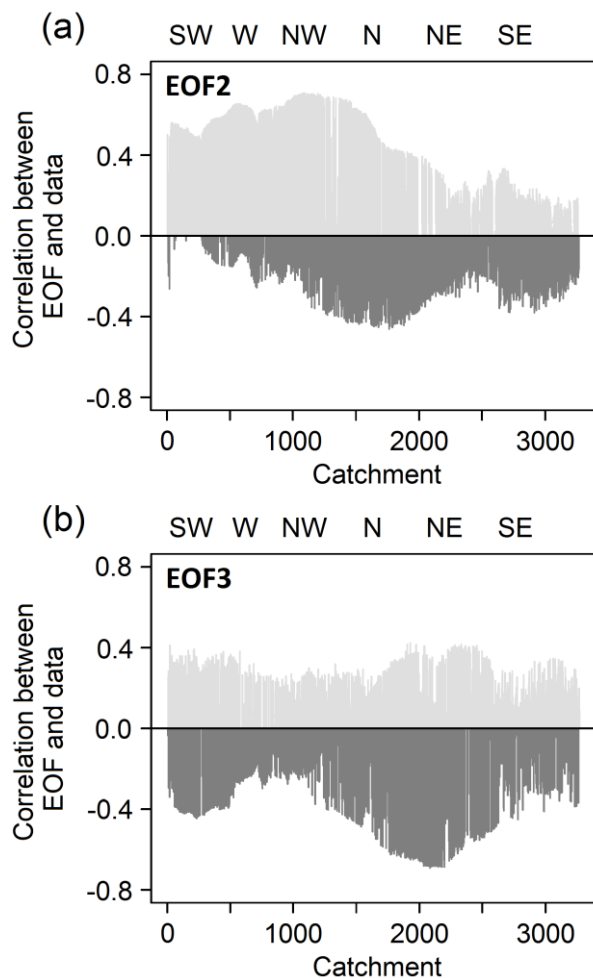
1199  
1200  
1201  
1202  
1203  
1204  
1205  
1206  
1207  
1208  
1209  
1210  
1211  
1212  
1213  
1214  
1215  
1216  
1217  
1218  
1219  
1220  
1221  
1222  
1223  
1224  
1225

1226 **Supplementary Material**  
1227



1228  
1229  
1230 **Figure S1:** SnowModel ERA-I simulated runoff time series (1979–2014) of the empirical  
1231 orthogonal functions (black curve) and 5-year running mean smoothing line (red curve) of EOF2  
1232 and EOF3. The explained variance is shown for each EOF. Both EOF2 and EOF were  
1233 insignificant.

1234  
1235  
1236  
1237  
1238  
1239  
1240  
1241  
1242  
1243  
1244  
1245  
1246  
1247



1248  
 1249 **Figure S2:** Eigenvector correlation values for each simulated catchment (1 to 3,272) for: (a)  
 1250 EOF2 and (b) EOF3. From left to right on the lower x-axis the catchments follows the clockwise  
 1251 path from the southern tip of Greenland (Southwest Greenland, Catchment 1) to the northern part  
 1252 (N section) and back to the southern tip (Southeast Greenland, Catchment 3,272). The location of  
 1253 the major regions: SW, W, NW, etc., are shown on the upper x-axis.